Fault Detection Using the Phase Spectra from Spectral Decomposition

A Thesis Presented to

the Faculty of the Department of Earth and

Atmospheric Sciences

University of Houston

In Partial Fulfillment

of the Requirements for the Degree

Master of Science

By

Umberto Barbato

December, 2012

Fault Detection Using the Phase Spectra from Spectral Decomposition

Umberto Barbato

APPROVED:

Dr. John Castagna
Chairman

Dr. Evgeni Chesnokov

Dr. Oleg Portniaguine

Dr. Mark A. Smith
Dean, College of Natural Sciences and Mathematics

Acknowledgements

Foremost I would like to express my sincere gratitude to my advisor Dr. John Castagna; his motivation and immense knowledge guided this research to what it has become today. His leadership has (and continues to) shape me into the professional that I am today.

Besides my advisor, I would like to thank my committee: Dr. Oleg Portniaguine and Evgeni Chesnokov, for guiding me during this process and providing me continuous support through the entirety of it.

I would also like to thank Carlos Moreno, Gabriel Gil, Charles Puryear, and Stu Fagin. They have helped me complete this research by providing council in different aspects of it.

Lastly, I would like to thank my family. My parents Roberto and Mariela Barbato, and brother Marco Barbato, for their personal and unconditional support through this entire effort.

Fault Detection Using the Phase Spectra from Spectral Decomposition

An Abstract of a Thesis Presented to

the Faculty of the Department of Earth and

Atmospheric Sciences

University of Houston

In Partial Fulfillment

of the Requirements for the Degree

Master of Science

By

Umberto Barbato

December, 2012

Abstract

Lateral changes in seismic phase can be used to detect small changes in seismic arrival time and waveform shape, independent of seismic amplitudes. A method to detect subtle seismic discontinuities, as may result from small-throw faults, using spectral decomposition phase spectra and a frequency-dependent phase attribute, derived from a combination of other structural attributes, is formulated. The application of this method to 3D synthetic models shows its dependency to signal to noise ratio. The composite attribute is later applied to seismic data from the Stratton and Hitts Lake fields. Both areas show complex faulting, which is efficaciously detected by the composite attribute. This attribute appears to outperform other commonly used attributes, like coherence and curvature, in characterizing faults, both vertically and laterally. Finally, the technique is validated by observing faults detected at well log scale.

Contents

List of Figures

List of Tables

Chapter 1

Introduction

1.1 Motivation for Present Work

In this research we will focus on the detection of faults. Fault picking is an important step in the process of reservoir characterization because faults are a hydrocarbon trapping mechanism. Understanding the fault system allows us to better measure our reservoirs statistics and better locate possible prospects. At the same time, leaky faults generate a problem of hydrocarbon retention, which is why it is very important to properly characterize them.

When it comes to exploration, one of the longer lasting tasks is interpretation of seismic data. Traditionally, interpretation was done by hand, a time consuming process. Several techniques have been developed in order to shorten this time, like the use of different seismic attributes.

The use of seismic attributes has a sizeable economic impact by saving time during the interpretation and exploration process. According to Randen (2011), "oil companies have suggested that for each 6 months saved, 5 % of the total cost of the development of the oilfield is saved". It is also important to take into account that a quick and well developed interpretation can better position a company when bidding negotiations take place.

1.2 Research Objective

Our main objective is to determine an automated yet effective attribute to efficiently delineate faults. The goal of an automated technique is to ease the task of picking faulting events by interpreters.

Another goal of this research is to improve on methods that are already commonly used in the industry. This is why the effectiveness of the technique is important. We strive for achieving better results than what is already available, while also aiming for more accurate responses.

The effectiveness of the attribute will be measured by how well it locates faulting and how it detects vertical and lateral extent of these discontinuities when compared to commonly used attributes in the industry.

The following sections describe the geologic background of the study areas and the data used for this study. These areas include two fields: the Stratton Field and the Hitts Lake Field.

1.3 Stratton Field Location

The Stratton Field is part of the Frio Formation, located in the south western part of Texas. Figure 1, from Levey (1994), shows the location of the Frio Formation in Nueces and Kleberg Counties. It also shows the location of the Stratton Field, at the northern section of the Frio Formation.

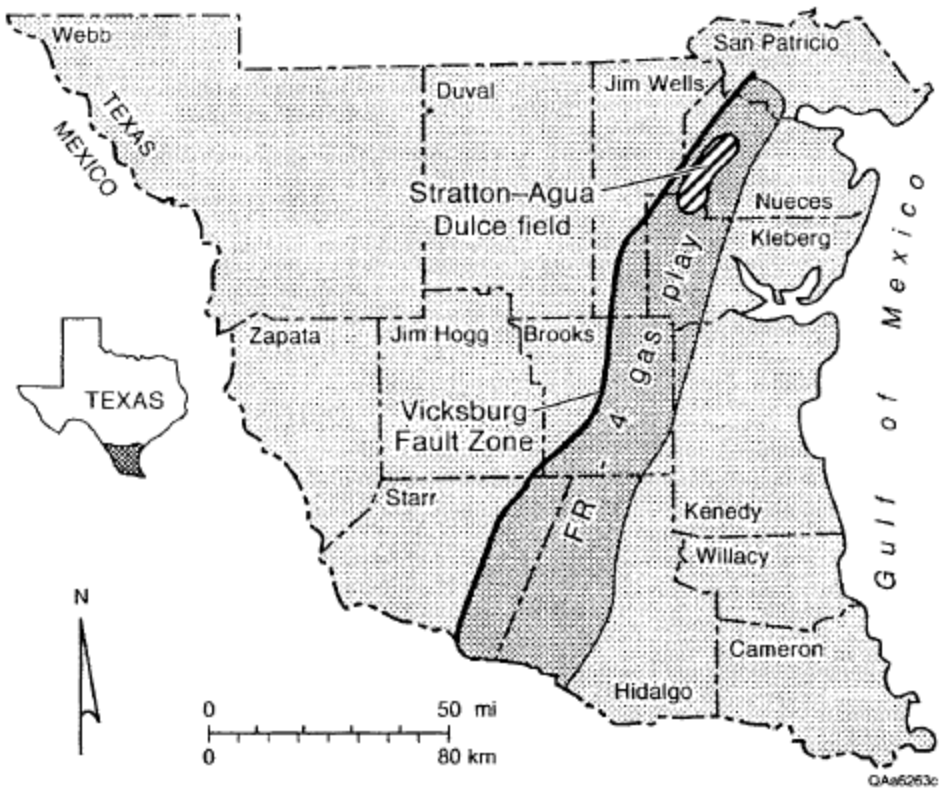

Figure 1. Base map showing the location of the Frio Formation and the Stratton Field (from Levey, 1994).

1.4 Geologic Background

As Levey (1994) states, "The Oligocene Frio Formation is one of the major progradational off-lapping stratigraphic units in the northwest Gulf Coast Basin". Figure 2 shows a schematic of the depositional sequences present in the Texas Gulf Coast Basin, where the Frio formation is observed. It shows that the depositional style of the Frio Formation is characterized by the deposition of sediments that are mostly supplied by the Rio Grande Embayment.

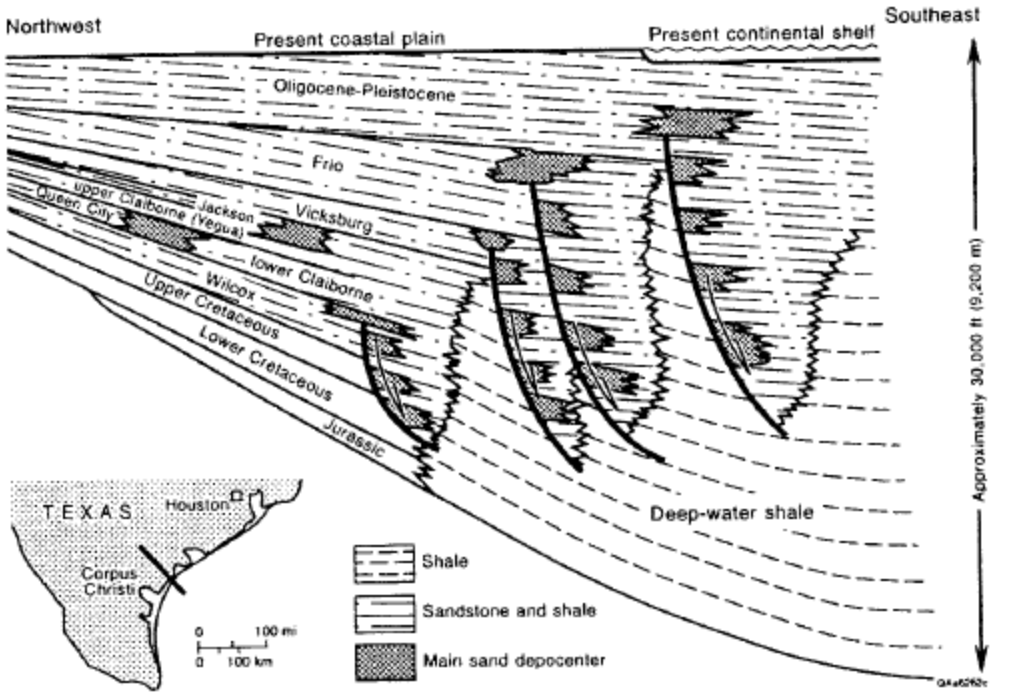

Figure 2. Schematic showing the depositional cross section of the Frio Formation (from Levey, 1994).

The Frio Formation is one of the largest gas plays in the Gulf Coast, as shown in figure 3. Over 12 TcF of gas had been produced up to 1991; and according to PESA (2001), the Stratton Field proved reserves are approximately 63.8 MMboe (approximately 0.010 TcF).

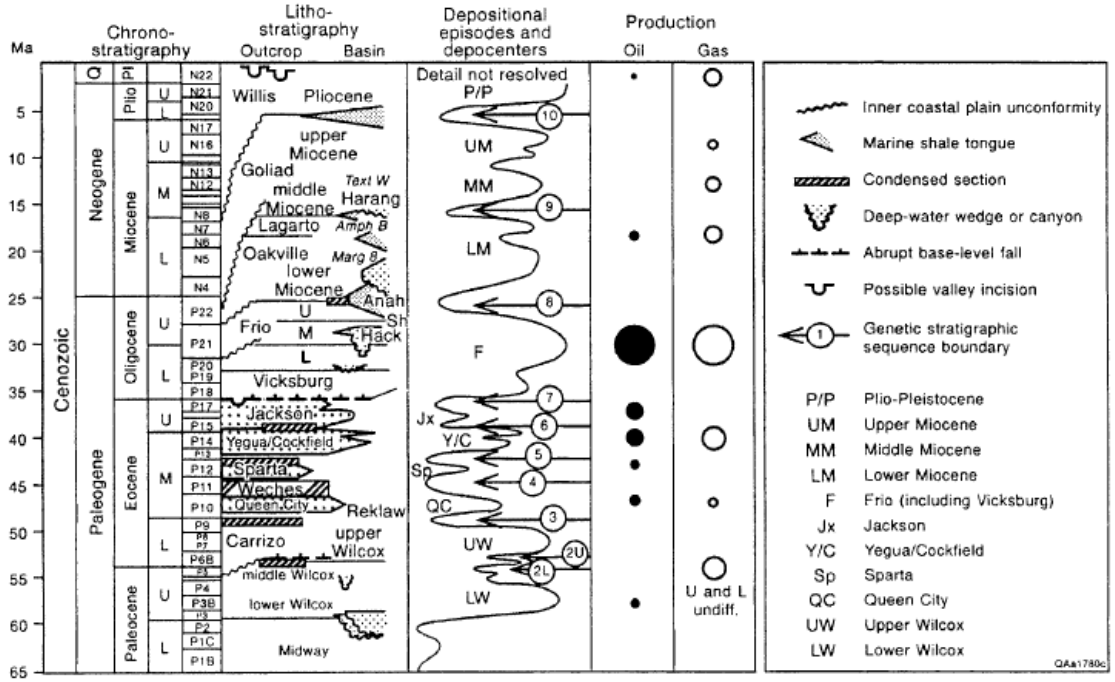

Figure 3. Stratigraphic columns showing volume of gas in the various formations in South Texas (from Levey, 1994).

The main trapping mechanisms in the formation are of both structural and stratigraphic nature. The main trapping features are combinations of closing faults, stratigraphic pinch-outs, and facies changes.

The Stratton Field is one of the several fields present in the Frio Formation. It extends from the Frio Formation to the top of the Vicksburg Formation. It is characterized by listric normal faulting (as seen in figure 2) with a series of antithetic faults, which compartmentalize the formation into smaller pockets. These laterally constrained beds are approximately from 10-15 feet thick, and as thick as 30 feet.

This complex structural setting makes reservoir characterization particularly important in order to maximize production in this area.

1.5 Stratton Field Data

The Stratton Field data are summarized in table 1. The location of the wells is observed in figure 4.

Seismic Data Set		
Data Set	**Bin Size (feet)**	**Area (Square miles)**
Stratton Field	110 * 55	9.18
Well Data Set		
Number of wells	**Well Logs**	
21	Induction, Caliper, Density, Gamma Ray, Neutron Porosity, Induction.	

Table 1. Data for the Stratton Field.

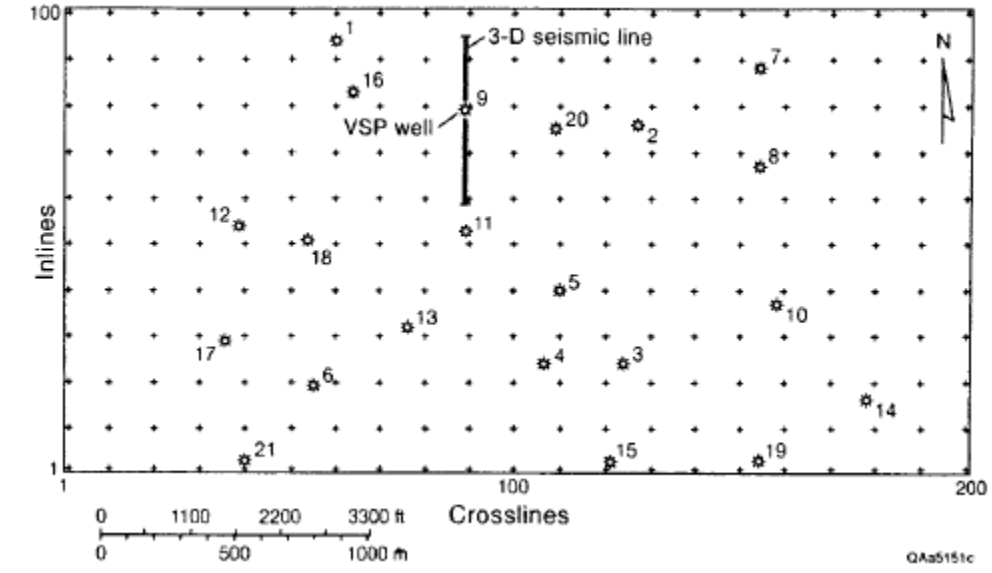

Figure 4. Locations of wells in seismic data (from Levey, 1994).

1.6 Hitts Lake Field Location

Hitts Lake field is located in the Smith County, in East Texas as shown by Figure 5, from Caughey (1977). The Paluxy Formation is one of the productive formations encountered in the field. Outcrops of this formation are also observed in figure 5, at the western most end.

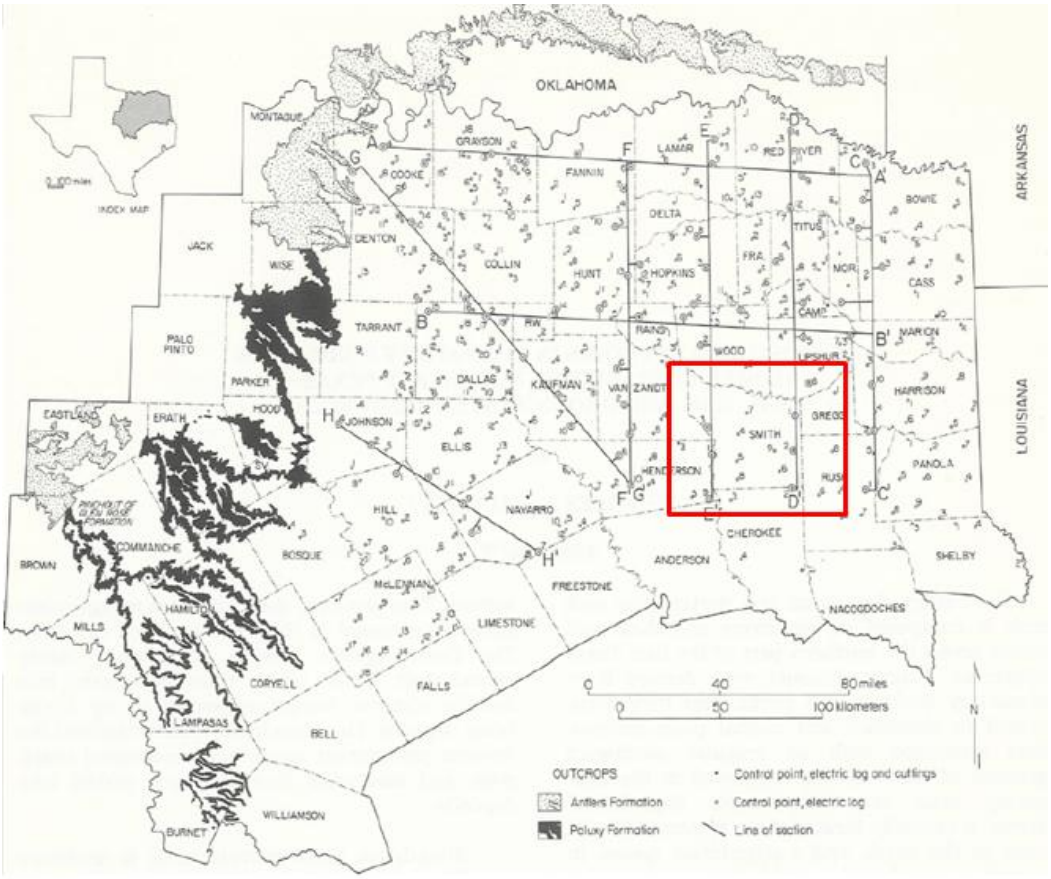

Figure 5. Location of Smith County and outcrops of the Paluxy Formation (modified from Caughey, 1977).

1.7 Geologic Background

"The Paluxy Formation was deposited in the broadly subsiding East Texas embayment, an inlet in the Gulf basin localized by a flexure of the Ouachita foldbelt" as stated by Caughey (1977). As it is observed in the outcrops, the Paluxy Formation thins southwards as a consequence of the Central Texas area being a less stable platform.

The structural framework is related to salt domes and normal faulting. Jackson (1982) explains that rifting during the Mesozoic, in combination with subsidence of the East Texas Basing, generated normal faulting parallel to the Ouachita Belt. This normal faulting formed the grabens observed in the basin. These grabens are defined by the Mexia-Talco Fault Zone, shown in figure 6.

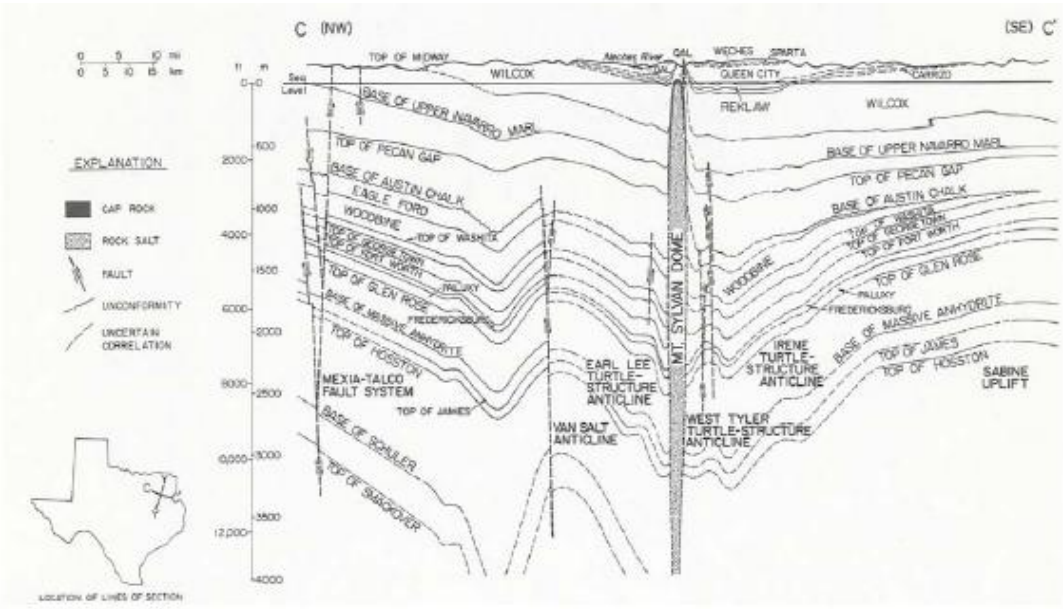

Figure 6. Mexia-Talco fault zone (from Jackson, 1982).

Figure 7 shows a model of the grabens present, as observed in a seismic cross-section.

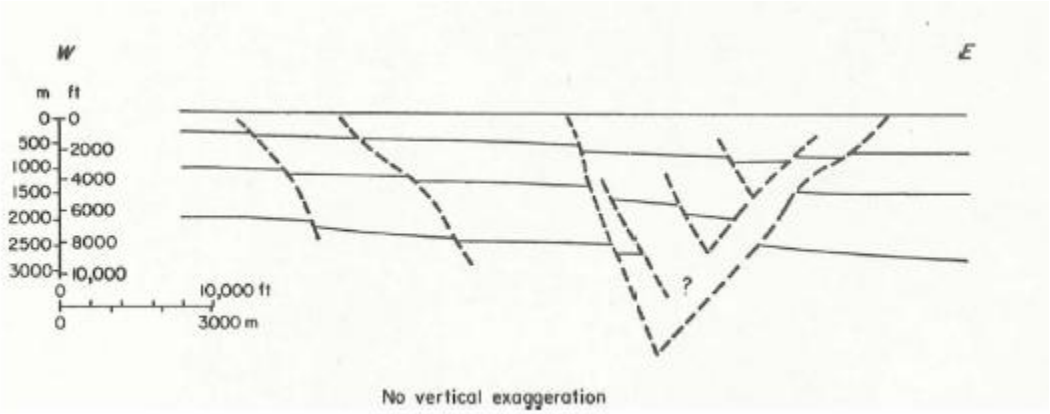

Figure 7. Graben model (from Jackson, 1982).

Other structures present are salt-related anticlines. Figure 8 shows salt diapirs, pillows, and turtle structures related to the Paluxy Formation.

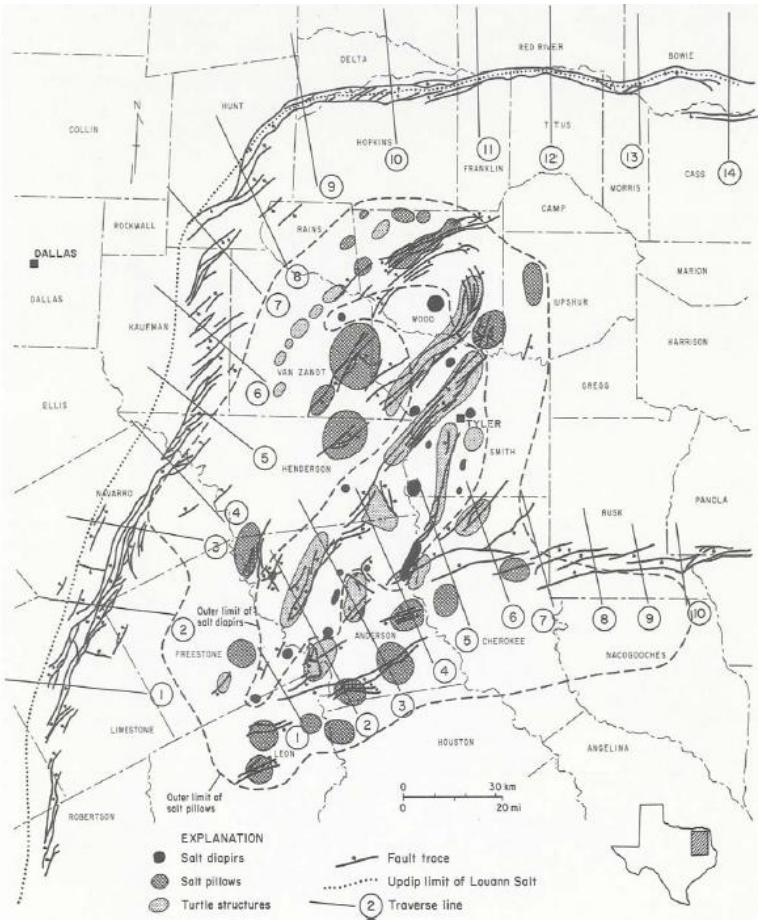

Figure 8. Salt-related structures observed in the Paluxy Formation (from Jackson, 1982).

Sourced by Upper Jurassic rocks, the Paluxy Formation has produced over "429 million barrels of oil and approximately 50 million MCF of natural gas" according to Caughey (1977). Figure 9 shows the resources observed in the Paluxy Formation.

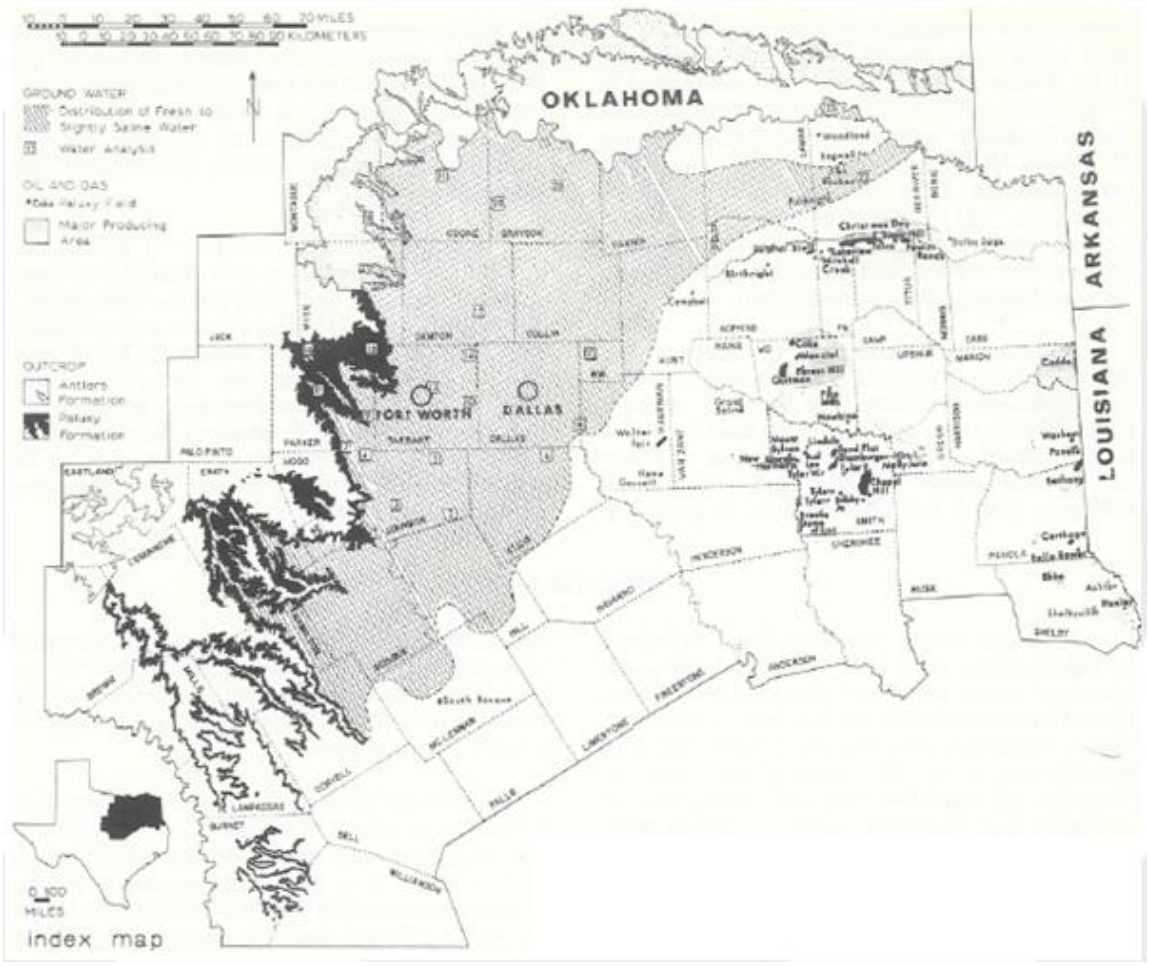

Figure 9. Map of resources from the Paluxy Formation (modified from Caughey, 1982).

1.8 Hitts Lake Field Data

The Stratton Field data are summarized in table 2. Figure 10 shows the location of the wells in the Tortuga Grande Survey. The blue polygon delimits the area where wells that penetrate the Hills Lake Field are clustered.

Seismic Data Set		
Data Set	**Bin Size (feet)**	**Area (Square miles)**
Tortuga Grande	110 * 110	26.8
Well Data Set		
Number of wells	**Well Logs**	
43	Induction, Caliper, Density, Gamma Ray, Neutron Porosity, Induction.	

Table 2. Data for the Hitts Lake Field.

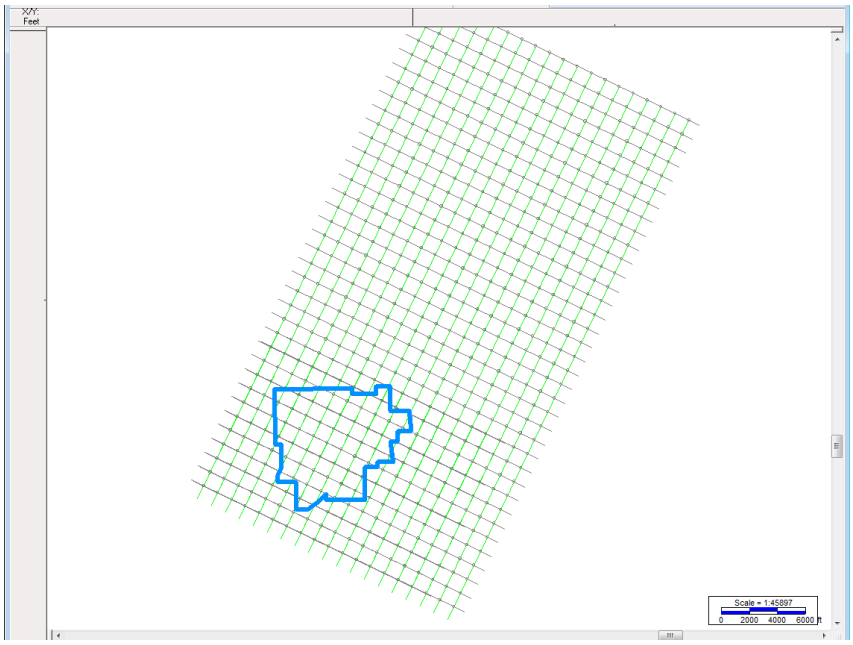

Figure 10. Location of wells in the Hitts Lake Field.

1.9 Conclusions

The Stratton Field, located in Nueces and Kleber Counties, in South Texas, is one of the largest gas-bearing formations in the area. It is affected by listric faulting, like the

Vicksburg Fault. Listric faulting (and its respective antithetic faults) form compartments that become important trap mechanisms for these hydrocarbons.

The Hitts Lake Field presents a series of grabens generated by normal faults. Known as the Mexia-Talco fault zone, these gravity-related features are generated by subsidence of the East Texas Basin with respect to the Ouachita Belt, and are located in Smith County, East Texas.

The goal of this thesis is to adequately detect these faults (with different structural origins) by applying an automated, yet effective, technique.

Chapter 2

Fault Detection Attribute

2.1 Introduction

Many techniques are applied in order to determine stratigraphic boundaries. Luo (1996) explains that seismic edge detection uses different attributes to determine boundaries and other discontinuities, like faults or fractures. Some of these include the use of geometrical attributes like coherence (as explained by Peyton, 1998), chaos, and curvature. These attributes are usually applied to the amplitude data.

Browaeys (2009) uses the instantaneous phase of the seismic data to determine stratigraphic boundaries. The continuous instantaneous phase is related to the continuity of the data and jumps on the phase show discontinuities on the subsurface. Because signal attenuation only affects the seismic amplitude, the use of the phase component allows us to observe events that might be lost in the amplitude spectra. Also, as Browaeys states, "phase variations are sharper and faster than amplitude variations".

Spectral decomposition allows us to study the seismic response at different frequencies, as explained by Puryear et al. (2012). The particular response at each frequency helps us determine stratigraphic boundaries, hydrocarbon presence, and provides resolution improvement when the data are being processed. Peyton (1998) uses the amplitude spectra of spectral decomposition in combination with other attributes, like coherence, to detect faults. This has proven to be a very useful technique.

However, very little has been done with the phase spectra obtained from spectral decomposition. Zhou (2007) uses the phase from spectral decomposition with the local structural entropy to enhance subtle discontinuities.

The use of the frequency-dependant phase spectra of the seismic data can give us a better insight when trying to detect discontinuities. It will also allow us to better characterize each fault, since faults behave differently at different frequencies. Furthermore, the combination of these frequency-dependant phase cubes with other edge-detecting attributes (like chaos or coherence) can help us enhance the detection of faults.

2.2 Workflow

The workflow for the proposed attribute consists of several steps.

Data conditioning might be necessary in order to improve signal to noise ratio. Since some of these attributes are very susceptible to noise, the less noisy our data are, the more accurate will be the response of these attributes. If the original dataset is very noisy, some of the steps of the workflow will highlight this noise (Edge Enhancing Attributes calculations), and some will reduce it (principal component analysis).

The workflow is divided in the following steps:

- Conditioning the data,
- Producing frequency dependant phase spectra by applying spectral decomposition to the original seismic data,
- Determining the frequency dependant phase spectra that will better achieve the objective of the project,

- Calculating various edge enhancing attributes on these various phase spectra,
- Applying principal component analysis, with the previously calculated attributes as the input parameters,
- Applying post-principal component analysis filtering.

2.3 Data Conditioning

In order to sharpen the effect of the phase spectra, the amplitudes are normalized by the following procedure. The envelope of the seismic data is calculated, and the trend of the envelope is determined by applying a low pass bandpass filter. The parameters of this filter are going to be dependent on the frequency bandwidth of the data, but in order to obtain the trend of the seismic data the first 10 Hz tend to be sufficient.

The next step will be to average each trace with its adjacent traces. This step normalizes the amplitudes.

The last conditioning step is to divide the previous result (normalized average amplitudes) by the envelope of the data. This last step will deliver a dataset with normalized amplitudes.

2.4 Spectral Decomposition (SD)

Taner (1979) explains that spectral decomposition is a method that allows us to study seismic responses in the frequency domain. The seismic trace's response is decomposed into different frequencies allowing us to analyze it in more detail.

Castagna (2003) uses the amplitude spectra of the spectral decomposition process to improve resolution, detect hydrocarbons, and better estimate thin beds. Partyka (1999) uses the phase spectra to determine geological discontinuities.

There are different methods of spectral decomposition. Some of them include the various Fourier Transforms (FT), Continuous Wavelet Transform (CWT), and Matching Pursuit decomposition (MP). Their differences are discussed by Castagna and Sun (2003).

As Puryear et al. (2012) state "the Short Time Fourier Transform (STFT) is based on the FT. which is equivalent to the cross-correlation of the seismic trace with a sinusoidal basis over a moving time window; the CWT, which is the cross-correlation of the seismic trace against a wavelet dictionary; and MP which is the decomposition of the seismic trace into basis atoms".

A novel method of spectral decomposition is the Constrained Least Squared Spectral Analysis (CLSSA). Like the Fourier Transform, it uses a series of sine and cosine functions to represent the seismic wavelet, but at the same time allows a priori information to be used as a constraint during the windowing process, allowing us to use small windows without sacrificing lateral resolution.

Puryear et al. (2012), show that the Short Time Fourier Transform results in frequency smearing, an effect of the introduction of a window in Fourier Theory. When introducing the window, the sinusoids are no longer orthogonal, allowing energy to "smear". The CWT provides poor resolution (varies in time and frequency depending on the side of the spectrum analyzed). The CLSSA provides excellent time and frequency resolution; it avoids the smearing problem by using a priori information to characterize

the edges of the window, effectively constraining the mathematical problem (by providing boundary conditions) and maintaining orthogonality between the sinusoids.

Figure 11 shows the performance of the Constrained Least Squared Spectral Analysis method next to the FT, CWL, and MP. We can observe that the CLSSA method closer approaches the real amplitude spectrum in all cases.

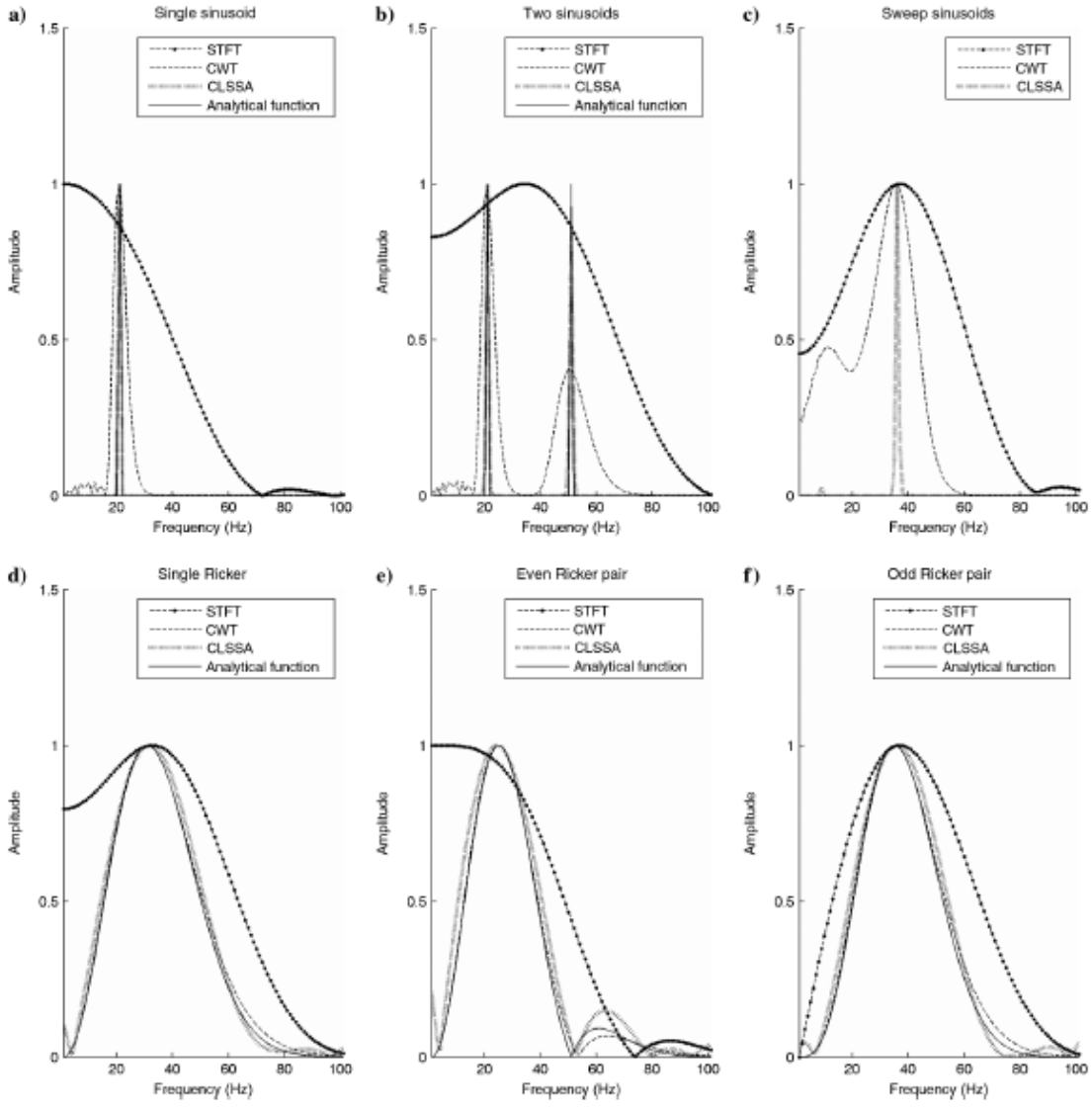

Figure 11. Comparison of results among all three methods (from Puryear et al. 2012).

The phase spectra will be used for the purpose of this study. Tanner (1992) emphasizes that discontinuities have sharper appearance on the phase of the seismic data; he also explains that the phase is not affected by signal attenuation.

It is important to note that the phase should be properly unwrapped. If phase unwrapping is not done properly (a mathematically complex process) stepping on the phase spectra can be observed. This effect shows small jumps along continuous events which might be perceived by the later used attributes as small discontinuities, which may translate to false faulting.

A helpful technique to avoid this problem is to use the cosine of the phase. The cosine of the phase allows us to rid the phase spectra of these jumps. At the same time, the cosine of the phase behaves like a short window Automatic Gain Control (AGC), which would also increase the noise level in the data. To avoid this final problem, the cosine of the phase is modulated by the envelope of the seismic. In the consequent steps, the modulated cosine of the phase spectra will be utilized.

2.5 Frequency Analysis

The frequency analysis consists on determining the best frequencies to use in the rest of the workflow. We limit the number of frequencies used because the computation of the complete workflow in all the frequency dependant phase spectra is an extremely time consuming exercise. Furthermore, the response observed in various frequencies might be similar among similar frequencies, so we limit the amount of frequencies used in order to be more efficient.

We observe the frequency behavior through the complete seismic broadband frequency in order to determine the best frequencies to use.

Frequency selection is going to be objective dependant. Major regional faults can be observed in the low frequency content of the spectrum, while smaller, more localized faults are better characterized by high frequencies.

The best way to determine which frequencies to use is to study the frequency dependant amplitude sections obtained from spectral decomposition. We observe these sections and try to determine which frequencies better characterize our target faults.

There is no limit on the number of frequency dependant phase spectra to use, but as the amount of sections used increases, so does computational time and weight (memory availability of a single workstation might become a factor at this point). This is one of the main reasons why the frequency analysis has to be carefully done; in order to be more efficient (without sacrificing on results quality) during the rest of the exercise. Seismic attributes are calculated after producing and electing the various phase spectra volumes to be used.

2.6 Edge-enhancing Attributes

Seismic attributes are considered to be any quantifiable characteristic obtained from seismic data. Taner (2000) provided a very comprehensive paper which lists and explains some of the main seismic attributes used. Several attributes are used specifically to improve resolution of seismic data and to enhance discontinuities. According to Taner, Instantaneous Phase is an excellent indicator of lateral continuity.

Some of the most common attributes used to enhance discontinuities are dip-guided. This means that the dip and azimuth of the structure are obtained before calculating these structural attributes, as Chopra (2008) formulates. Calculating the dip uses an automatically picked horizon and determines the surface of reflectors; as the dip map changes, discontinuities are measured. This technique is applied in the calculation of geometrical attributes, such as coherence.

2.6.1 Coherence

The coherence cube was introduced by Bahoric and Farmer, and according to Chopra (2008), "measures similarity between waveforms or traces". It uses changes in impedance (as a reflection of the local geology) to determine changes in lithology, which is done by comparing the response of a seismic trace to the response of the adjacent traces.

Coherence is calculated by cross-correlating a target trace with its adjacent traces. If the waveforms are similar, then we observe a coherent event; when they differ, the event is incoherent. Incoherent events (like faults) are highlighted.

This attribute is also affected by dipping beds. Dipping events are incoherent at trace level because the traces are different at similar times (this is going to be dependant of the window size), therefore deeming continuous but dipping events, incoherent.

Figure 12 shows the response of the coherence attribute on a seismic section. Figure 12 (a) Shows a coherence time slice of the seismic time slice (b). Faults are highlighted by black and white arrows on the seismic section, and observed in the coherence cube.

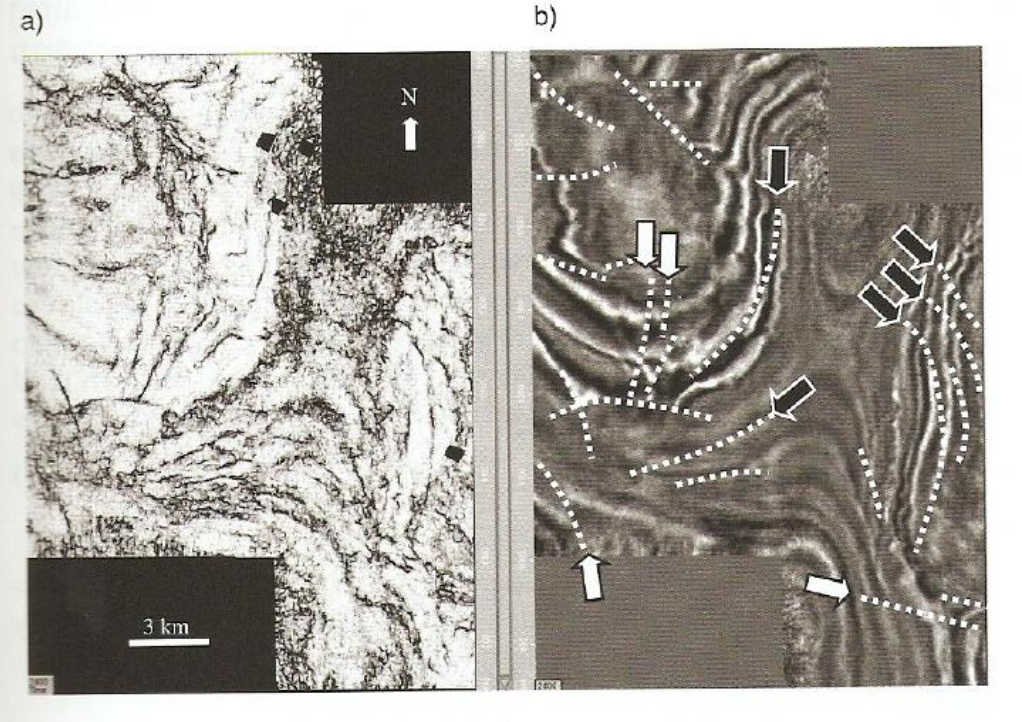

Figure 12. a) Shows a coherence time slice of seismic section b) (from Chopra, 2008).

2.6.2 Chaos

Chaos is a measurement of texture. It measures if the seismic signal behaves consistently with respect to an azimuth. Areas that do not behave consistently are rendered chaotic, and this effect is usually a response to faults, channels, and other types of discontinuities. Chaos is also dip-guided (while it doesn't use the dip component, it uses the azimuth component).

Each C-matrix contains three eigen vectors with their respective eigen values (λ). The largest eigen value (λ_{max}) is representative of the dip an azimuth of the event (this event is determined by calculating the local dip and azimuth, during the dip guidance step). As Randen (2011) explains, the difference between λ_{max} and the other two eigen values (λ_{mid} and λ_{min}) shows the level of "chaoticness" in the event.

Figure 13 shows some of the possible scenarios. Figure 13 (a) shows a continuous reflector, which will show a large difference between λ_{max} and the other two eigen values (which will be similar to each other). Figures 13 (b) and (c) show faulting scenarios, where the values of λ_{mid} and λ_{min} are going to be larger, and closer to λ_{max}, which would show large magnitudes of gradients with different orientations.

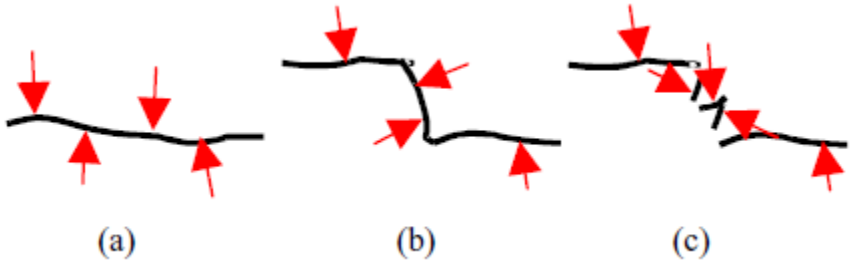

Figure 13. a) A continuous reflector will show $\lambda_{max} \gg \lambda_{mid} \approx \lambda_{min}$, b) a continuous (but bent) reflector will show $\lambda_{max} \approx \lambda_{mid} \gg \lambda_{min}$, c) a discontinuous reflector will show $\lambda_{max} \approx \lambda_{mid} \approx \lambda_{min}$ (from Randen, 2011).

Figure 14 shows an example of the chaos response applied to a seismic section. The Chaos time slice clearly highlights the faults in the section, but at the same time it also highlights noisy responses (as it is shown in the southwestern corner of the section).

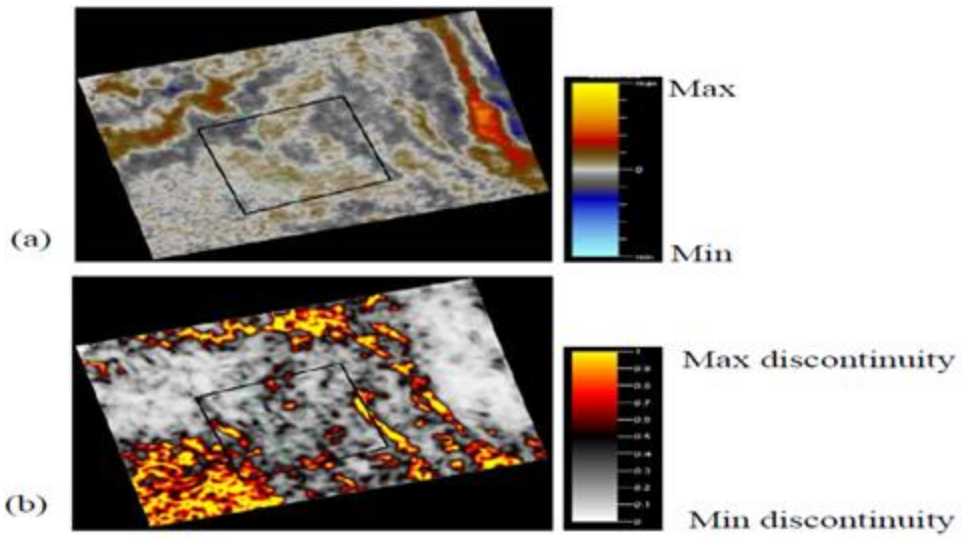

Figure 14. a) Seismic time slice. b) chaos time slice of (a) (from Jansen, 2005).

2.6.3 Most Positive Curvature

The curvature attribute is a popular attribute to map fractures, as used by Chopra (2008). According to Chopra, curvature is defined as "the radius to a circle tangent to a curve". Figure 15 shows graphically the definition of curvature in a two-dimensional plane.

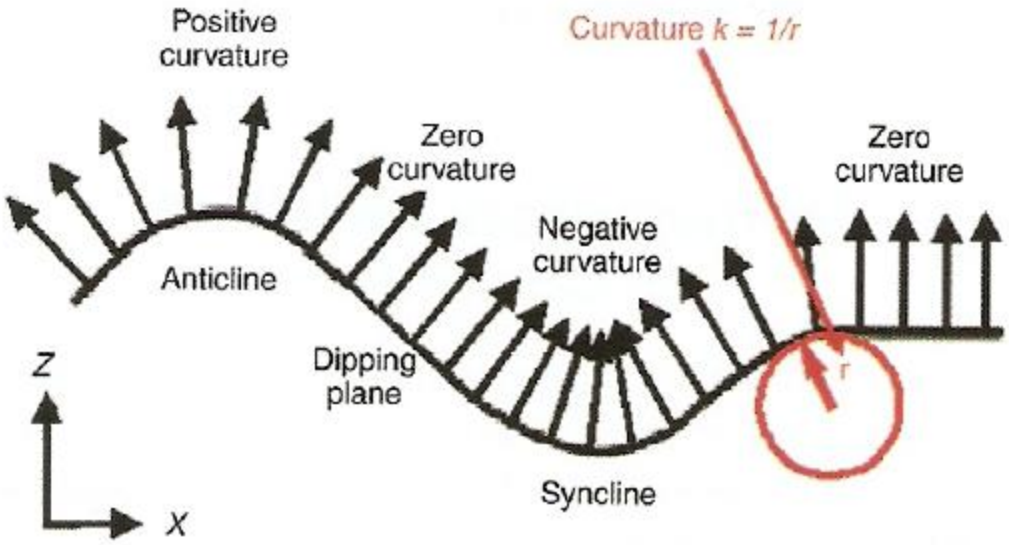

Figure 15. 2D representation of the definition of curvature (from Chopra, 2008).

It is clear from the literature that there are different types of curvatures that can be calculated. Some of these include Gaussian, both mean curvatures, most positive, most negative, along dip, along strike, etc.

All these various types of curvatures are calculated along a quadratic surface fitted to the horizon or event being analyzed. This surface, z(x,y), is mathematically expressed by

$$z(x,y) = ax^2 + cxy + by^2 + dx + ey + f.$$

One common type of curvature used for fault detection is most positive curvature. It is mathematically defined by

$$k_{pos} = (a+b) + [a - b^2 + c^2]^{1/2}.$$

The responses observed by both, most positive and negative curvatures, allow us to determine the geometry of the structure, since the most positive curvature can have

negative values and the most negative curvature can have positive values. Figure 16 shows the possible configurations observed when studying both attributes.

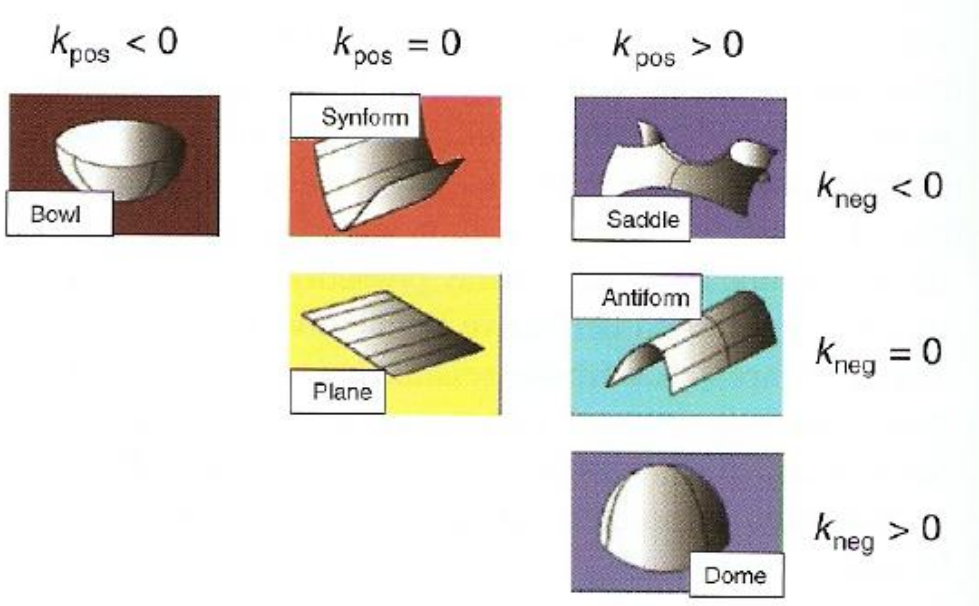

Figure 16. Possible configurations of structures observed by most positive and negative curvature (from Chopra, 2008).

Figure 17 shows the most positive curvature calculated over a seismic horizon.

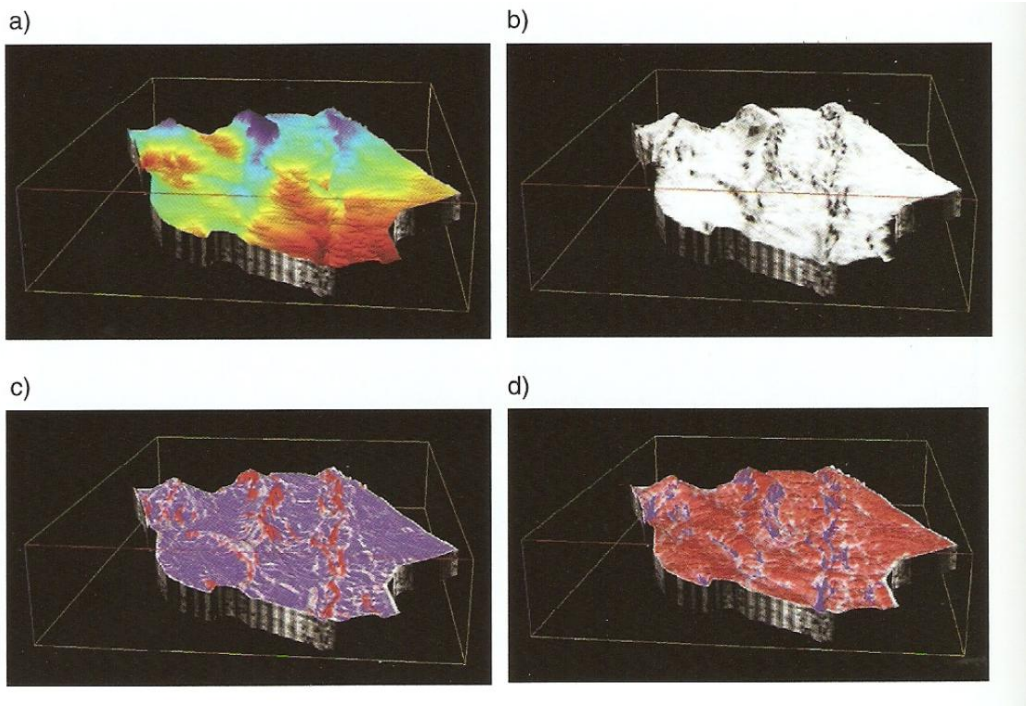

Figure 17. Comparison between a) a seismic horizon, b) coherence, c) most positive curvature and d) most negative curvature (from Chopra, 2008).

2.6.4 Variance

Another dip-guided attribute, variance is an attribute similar to semblance. As it is defined by Chopra (2008), semblance is "the ratio of the energy of the average trace to the average energy of all traces along a specified dip".

Figure 22 shows the steps in calculating semblance. Figure 18 (a) Shows the traces used to calculate the semblance (this traces are windowed). Figure 18 (b) shows the average energy of those traces. Figure 18 (c) replaces the traces in (a) with trace (b). Semblance is the ratio of (a) to (c).

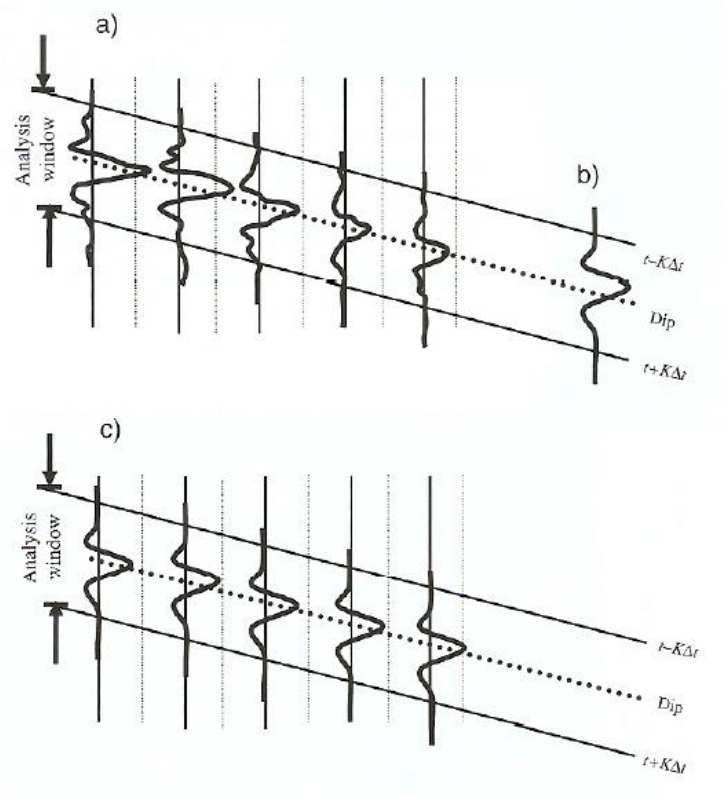

Figure 18. a) Energy of the traces used is calculated. b) The average trace is also calculated, and positioned to replace the original traces used in (a) to obtain (c). The ratio of (a) to (c) is the semblance (From Chopra, 2008).

Chopra goes on to explain that variance is simply one minus the semblance.

Semblance measures the energy similarity between the used traces and the average trace, while variance measures the dissimilarities between them. Figure 19 shows an example of the variance response applied to a seismic section.

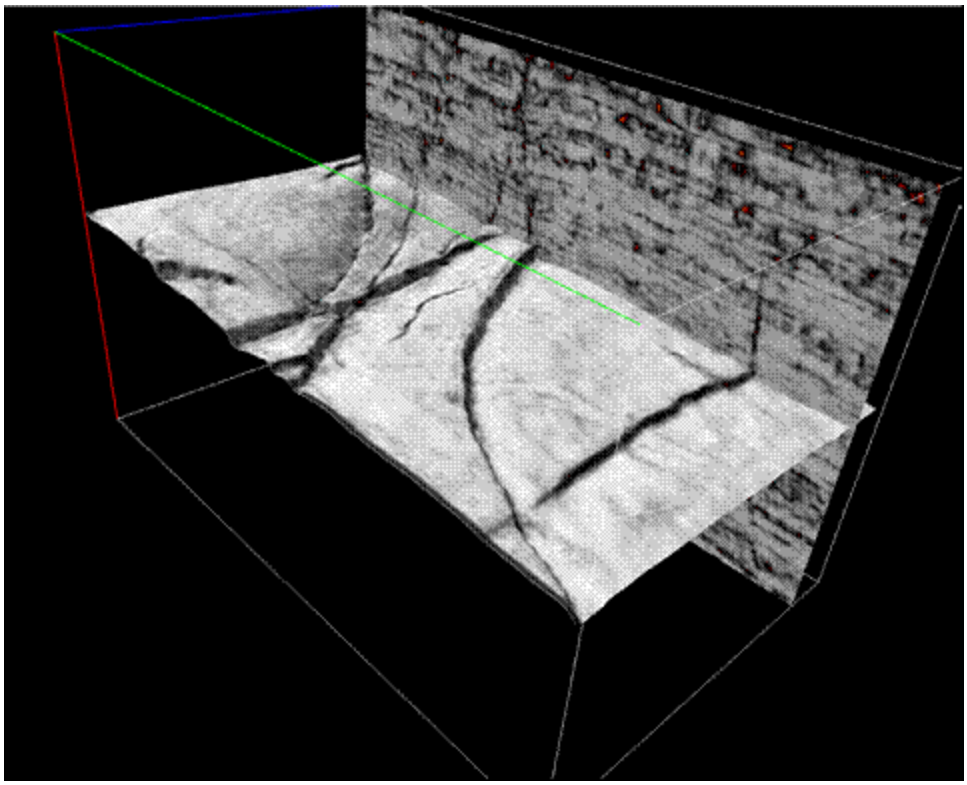

Figure 19. Example of a variance cube (from National Central University, 2005).

2.6.5 Laplacian Operator

The Laplacian operator is a mathematical operation applied to the seismic trace. Pujol (2003) defines it by the sum of second spatial derivatives of a vector *u*. It is described by the equation;

$$\nabla^2 \boldsymbol{u} = (\nabla^2 u_1, \nabla^2 u_2, \nabla^2 u_3);$$

when applied on a plane, it compares magnitudes of variations along that plane. For this study, the variations it will compare will be on the phase of the data; therefore small variations, which show semi-orthogonal derivatives, will have high valued responses which correspond to faulting. On the other hand large variations show semi-parallel derivatives, low valued responses, and correspond to dipping layers.

Figure 20 shows how the responses to the Laplacian operator are recorded (Randen, 2001).

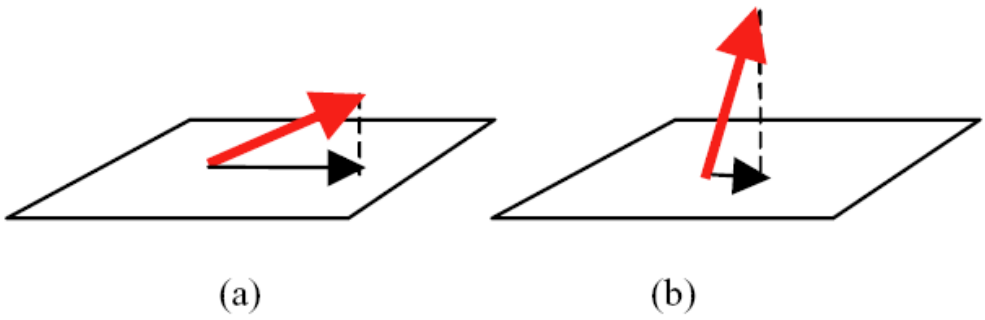

Figure 20. Vector derivative response. a) shows a semi-parallel response, typical of dipping layers; b) shows a semi-orthogonal response, typical of faults (from Randen, 2011).

2.7 Principal Component Analysis

As Guo (2009) states, "Principal Component Analysis finds a new set of orthogonal axes that have their origin at the data mean and that are rotated so that the data variance is maximized". Principal Component Analysis allows us to convert variables that are possibly correlated into linearly uncorrelated variables. An example is shown in figure 21.

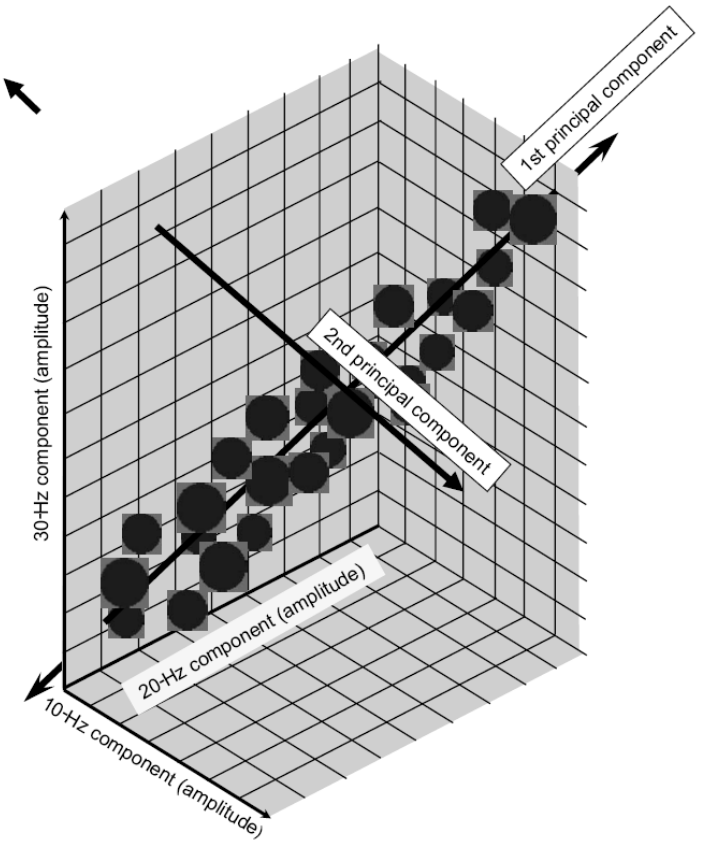

Figure 21. Example of Principal Component Analysis. Three principal uncorrelated principal components are obtained from three possibly correlated spectral components (from Guo, 2009).

In this case, spectral components are used as input variables. Three principal components are determined and orthogonal to each other (uncorrelated).

The difference between them is generated by data variability as result of having the components being uncorrelated. Therefore, most of the non-variant information tends to be observed in the first few components. The subsequent components tend to be the result of noise (which makes Principal Component Analysis an excellent tool to filter out noise in the data).

For this study, only the first few components are of interest. The invariant responses from the attributes are the discontinuities observed by them. The more variant

responses (later components) will be noise in the data and less constant features picked by the different attributes (which can be dipping layer responses).

2.8 Conclusions

The detection of subtle discontinuities has been a topic of discussion since it allows us to better characterize them. The use of frequency dependent panels obtained from spectral decomposition allows us to observe the response of these discontinuities at various frequencies, permitting us to better observe the behavior of these features. Furthermore, the use of the phase spectra (instead of the more commonly used amplitude spectra) gives us a tool to better observe these subtle changes in the seismic response, since they have sharper variations in the phase spectra. By better observing these changes in the phase spectra, and by applying the attributes discussed, we will construct a seismic cube that will present only our targets: the faults present.

This cube will show better resolution of these faults, which in turn allows us to better characterize the reservoir.

Chapter 3

Workflow Applied to Synthetic Models

3.1 Building the Synthetic Models

Twelve synthetic models representing a different fault in each were built.

The models were built using the Convolutional Model; we used normal incidence P-waves in an isotropic and homogeneous medium. The wavelets used were Ricker wavelets with frequencies depending on the corresponding model built.

Lastly, the models are sampled every 1 ms.

Models A, B, and C show faults of zero dip, and 10 ms throw. The dominant frequencies of these faults are 20, 30, and 40 Hz. They are also oriented in 45°, -45°, and 45°, respectively.

Models D, E, and F are similar to A, B, and C. Their main difference is that this set of models has a throw of 30 ms. Also; noise of about 5% (absolute) is introduced in these 3 models.

Models G, H, and I, are similar to A, B, and C. Their main difference is that this set of models is dipping by 0.65 ms/trace.

Lastly, models J, K, and L have zero dip and 10 ms throw. Their main difference is that they are all oriented in 0°.

These models will be arranged in a grid and built into a single seismic volume, to improve processing time. After gridding, the final grid will count with 204 inlines and 153 crosslines.

Figure 22 shows the grid of the models.

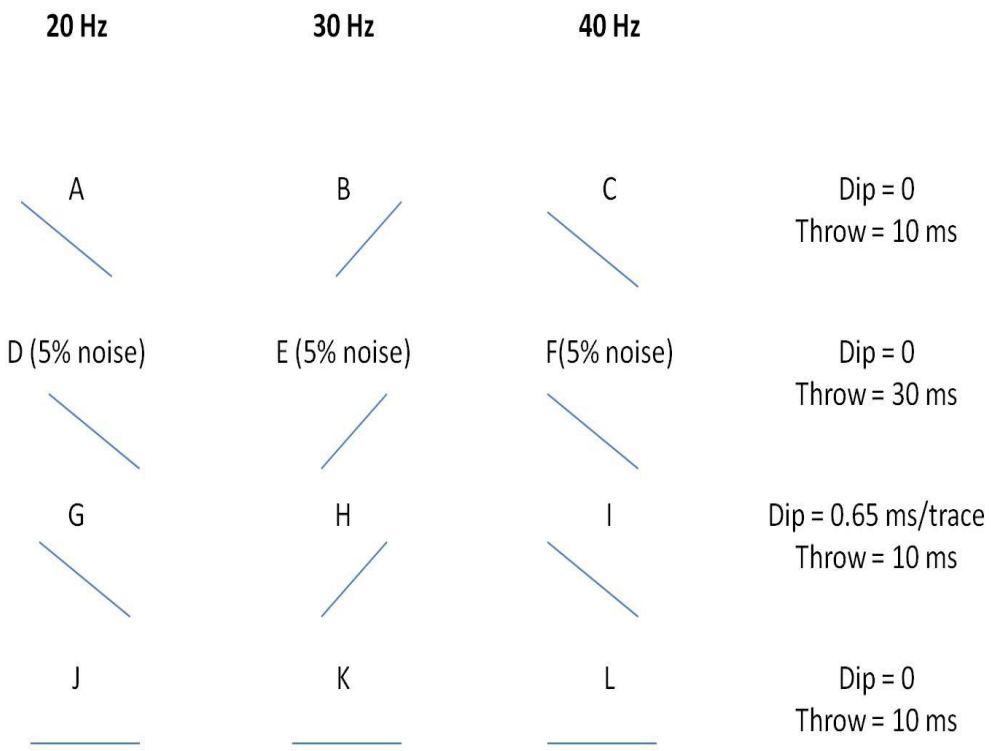

Figure 22. Grid of models used.

3.2 Application of Workflow to the Synthetic Models

The previously described workflow will be applied to the synthetic models. The following parameters will be used.

3.1.1 Parameterization

The preconditioning steps are mostly automatically parameterized. The frequencies used in the low pass bandpass are [-100, -50, 5, 10] (in Hertz). This will allow only the low frequencies from the right tail of the bandpass to be permitted through

the normalizing steps. The traces are averaged to their next 21 traces in both x and y directions.

Constrained Least Squared Spectral Analysis will be processed in all these models using a 20 ms window. The dominant frequency corresponding phase cubes (in this case 20, 30, and 40 Hz) will be analyzed.

To these cubes we will calculate several edge enhancing attributes. These include coherence, chaos, variance, most positive curvature, and the Laplacian operator. The attributes are applied with a vertical window of 9 samples and a lateral window of 3 samples.

The next step will be to apply Principal Component Analysis that will include the previously calculated attributes as inputs.

3.3 Results

The complete workflow is applied to the grid of models. Figures 23, 24, and 25 show time slices (time = 100 ms) the responses for coherence, most positive curvature, and the fault detection composite attribute.

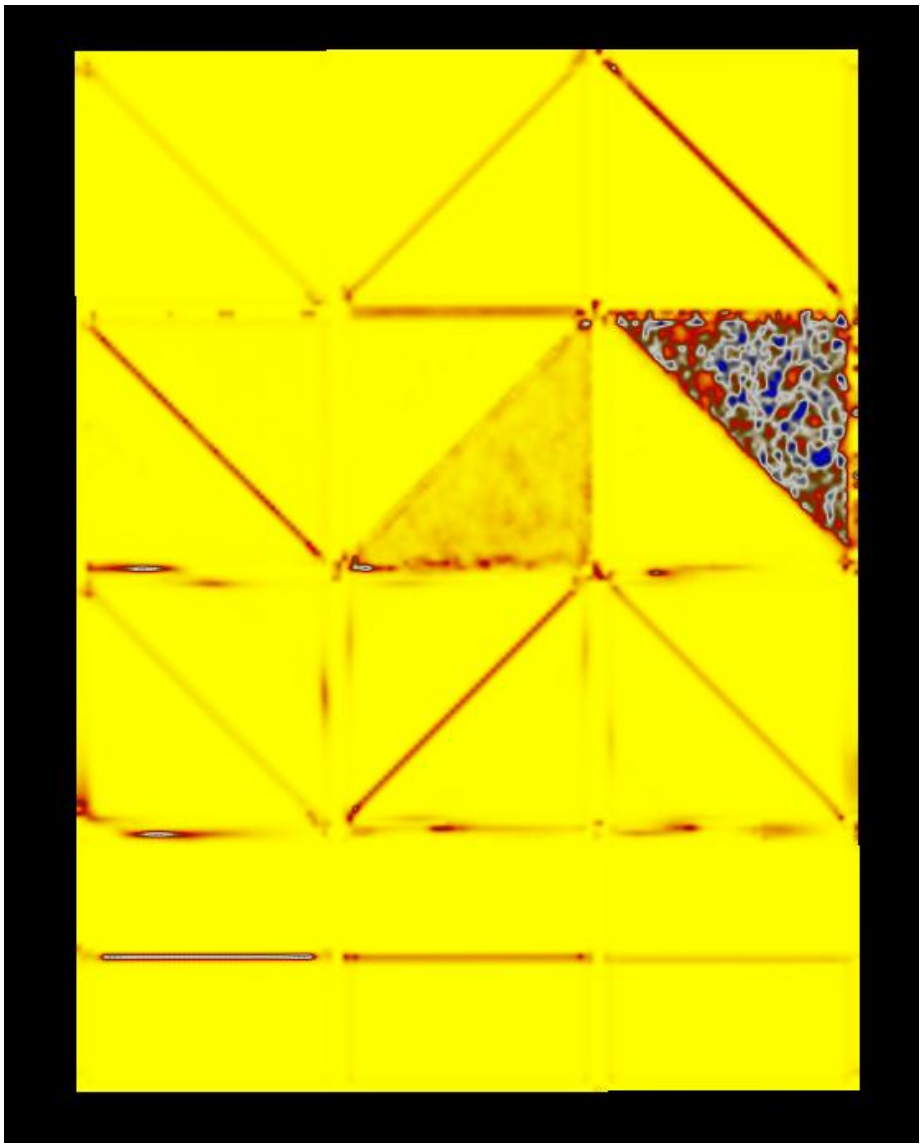

Figure 23. Time slice of coherence.

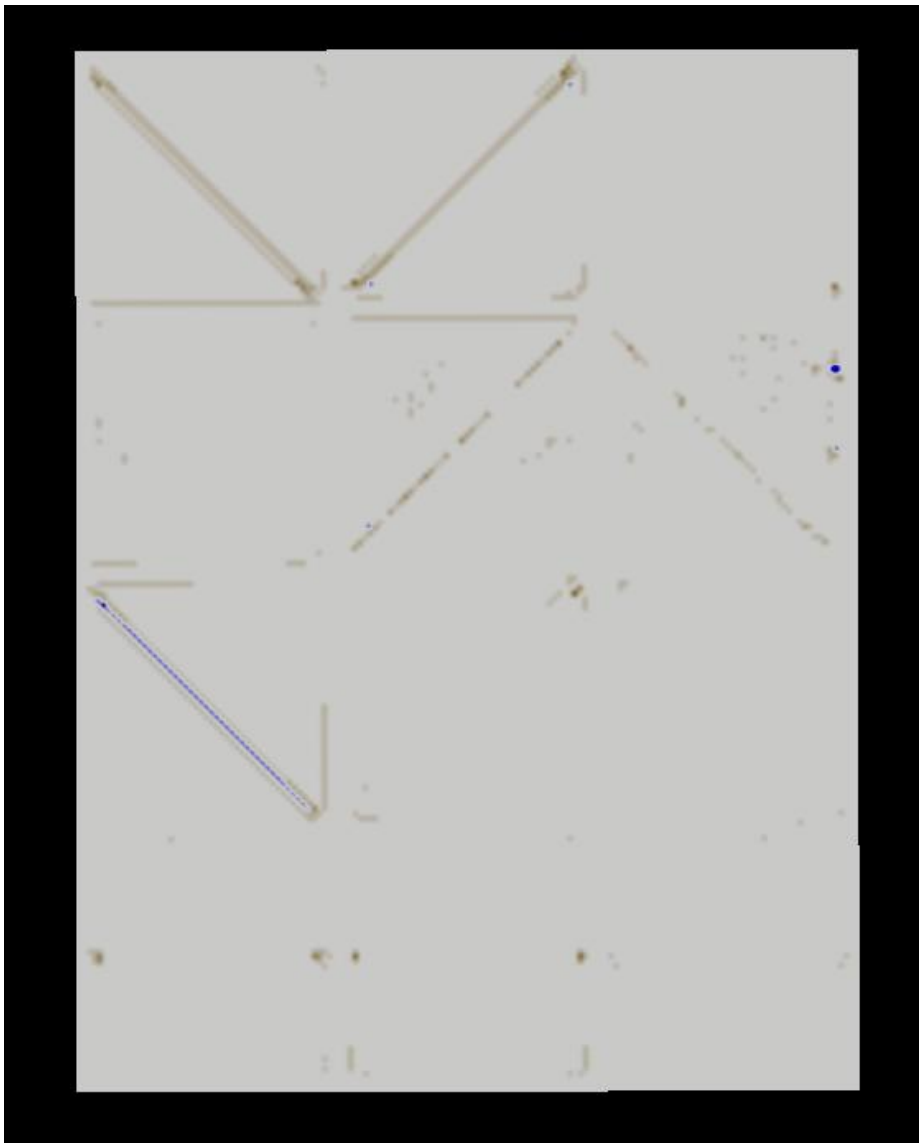

Figure 24. Time slice of most positive curvature.

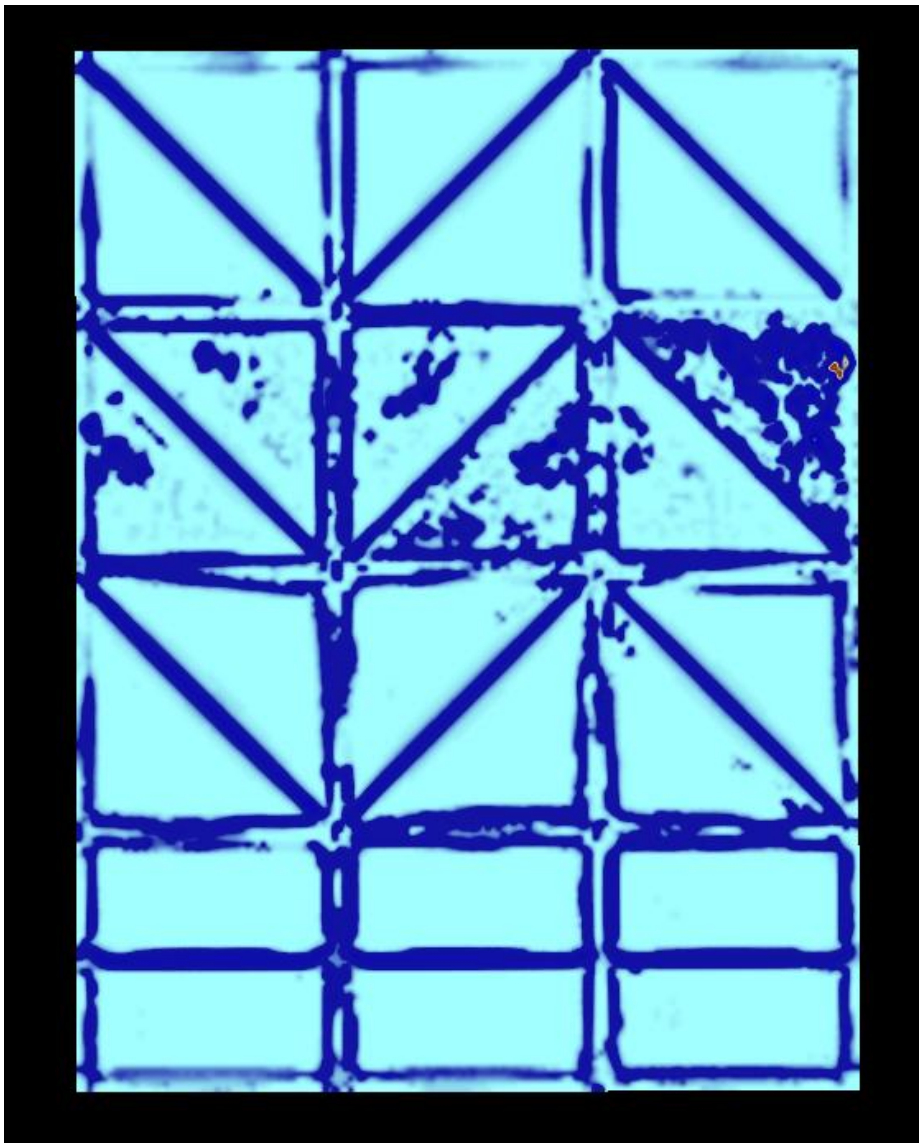

Figure 25. Time slice of composite attribute.

We can observe the difference between some of commonly used techniques (coherence and most positive curvature) and the composite attribute. The few artifacts observed in the method's response appear to occur only in the noisy and dipping fault data, so a structural filter was applied to the original data set and the workflow re-applied in order to observe the effect of noise in the workflow. The new result is shown in figure 26.

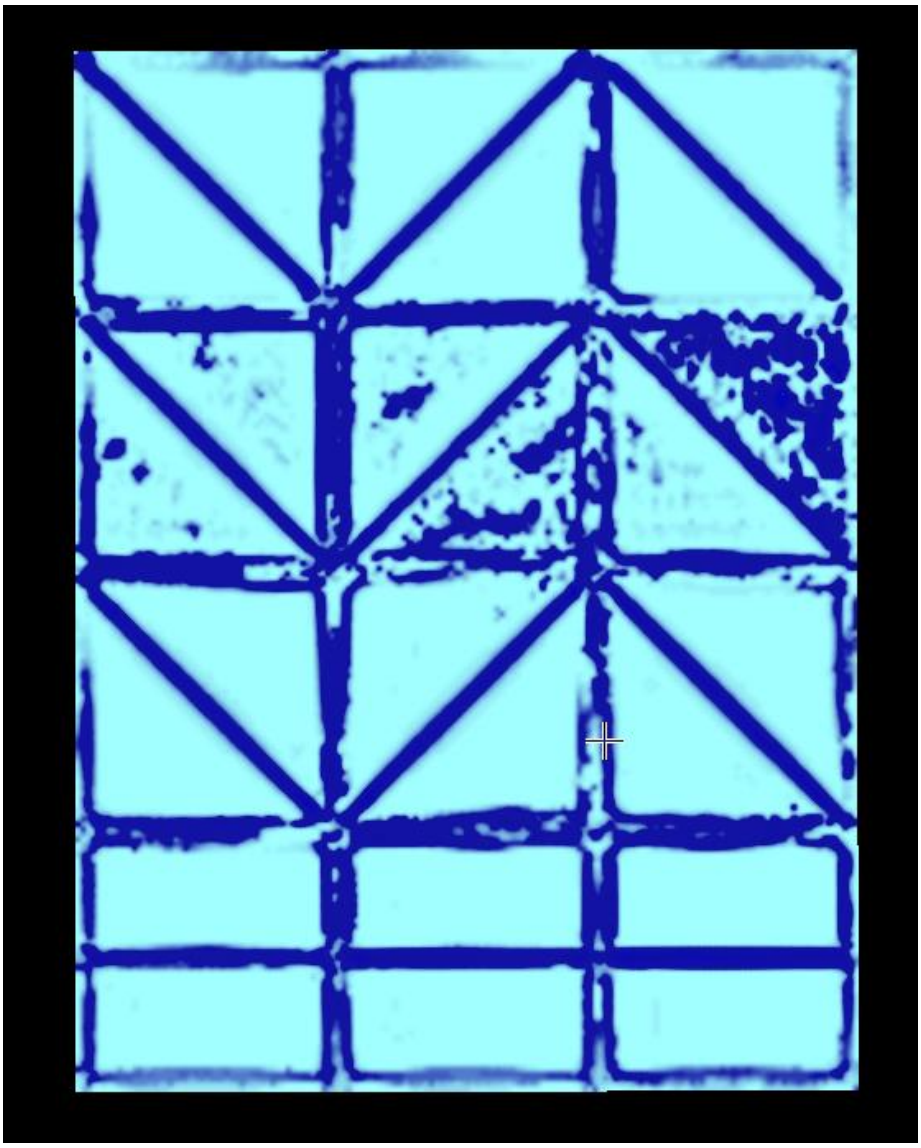

Figure 26. Time slice of the composite attribute after structural filtering.

3.4 Conclusions

We can observe that the composite attribute is superior to the conventionally used attributes when applied to these simple synthetic models.

Most positive curvature appears to have the least satisfactory response, picking the faults in some cases and not picking it in others (some because of the presence of noise and some because of dipping layers effects).

Coherence does an excellent job at picking the fault but it is highly affected by noise, an effect that worsens as higher frequencies are approached, which suggests that it would miss small features that would be hidden among high frequency noise.

The composite attribute appears to have the best response but it is affected by noise presence in a similar fashion as is coherence. After structural filtering, some absolute noise is removed. Improvement can be observed in the proposed technique after noise removal. The faults are picked with the least amount of artifacts.

Fault orientation, dip, and throw do not appear to be significant to the detection of the faults. The presence of noise appears to be the dominating factor.

This leads us to conclude that, while the proposed technique appears to be superior to the generally used attributes, it is also highly affected by the presence of noise.

Chapter 4

Composite Attribute Applied to Stratton Field Data

4.1 Application of Composite Attribute to Stratton Field Data

The composite attribute is applied to the Stratton Field seismic dataset. The focus study area lies inside inlines 1-155 and crosslines 1-230. The interest area also lies between 1300 and 4300 ms, where the Vicksburg listric fault is observed in the crossline direction. We can also observe its small antithetic faults which compartmentalize the onlapping section, as discussed in chapter 1. Figure 27 shows a cross section of inline 142, where we can clearly observe the listric fault.

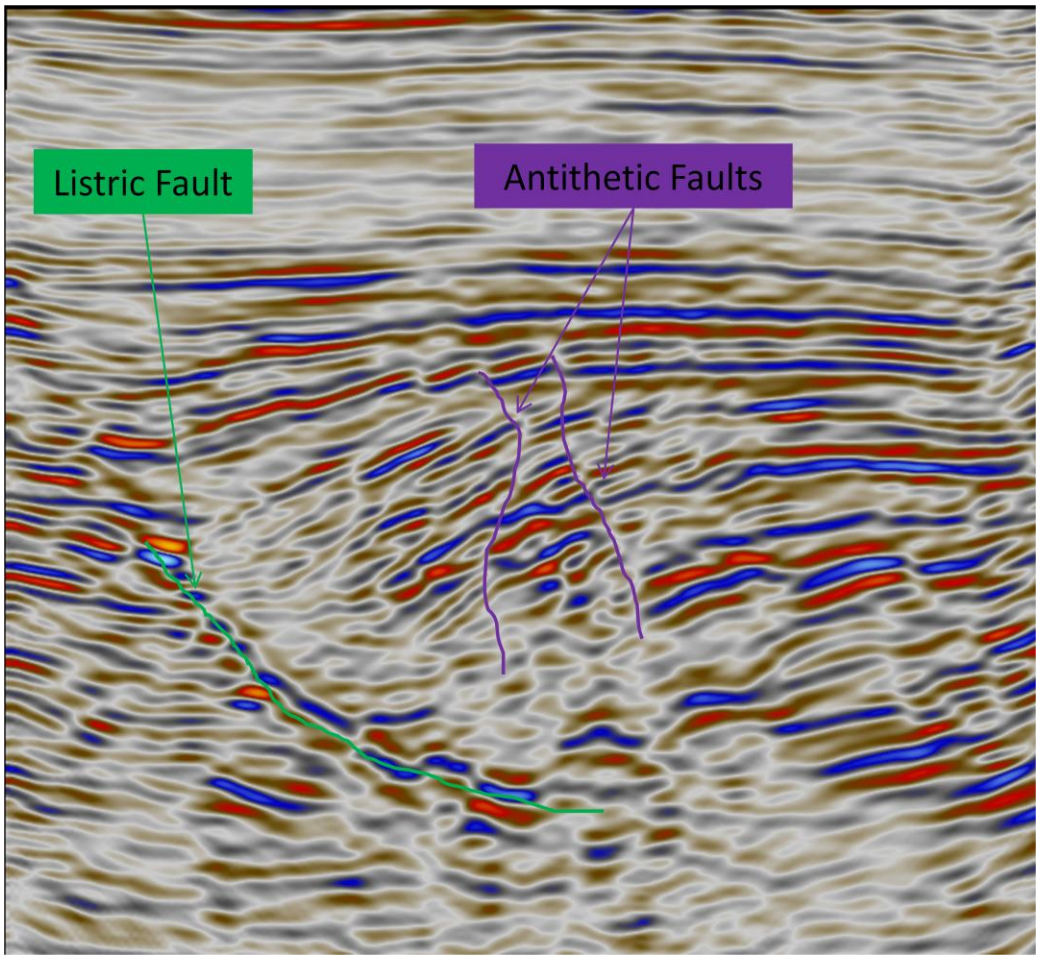

Figure 27. Inline 142 showing listric and antithetic faulting.

The objective of this project is to map all present faults. Based on this objective we inspect the amplitude spectrum of the data (observed in figure 28) and determine the frequencies to be used for the rest of the study. The frequency dependent amplitudes are then compared to determine if the chosen frequencies are the best characterizer of the geological features targeted to be mapped. The chosen frequencies are 20, 30, 50, a.70 Hz

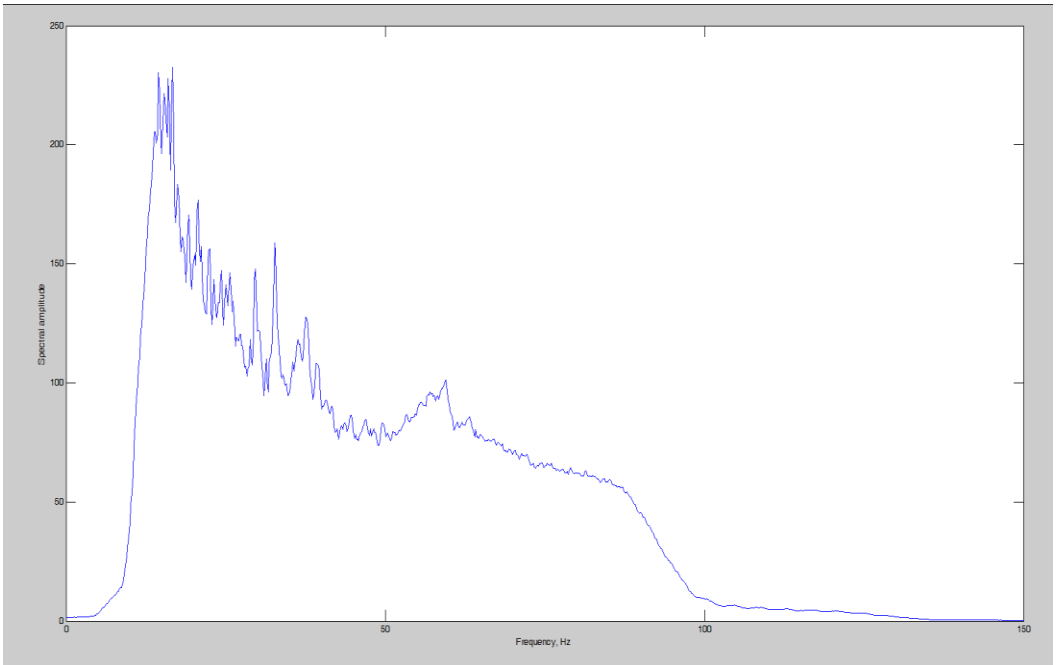

Figure 28. Average amplitude spectrum of seismic traces from the interest area.

4.1.1 Parameterization

Similar to the synthetic models, the preconditioning steps are mostly automatically parameterized. The frequencies used in the low pass bandpass are also [-100, -50, 5, 10] (in Hertz). The traces are averaged to their next 201 traces in both x and y directions.

Constrained Least Squared Spectral Analysis will be processed in Stratton Field seismic dataset using a 20 ms window.

We will apply several edge enhancing attributes to the selected frequency dependant phase spectra. These include coherence, chaos, variance, most positive curvature, and the Laplacian operator. The attributes are applied with a vertical window of 9 samples and a lateral window of 3 samples. The data is sampled at 0.5 ms (therefore the vertical window is 4.5 ms long).

The next step will be to apply principal component analysis that will include the previously calculated attributes as inputs.

4.2 Results

The results and original data were loaded into Petrel once the workflow was completed. Figure 29 shows the seismic response, instantaneous phase response, and the workflow applied to inline 142. More results, and the discussion of these, will be shown in the next chapter.

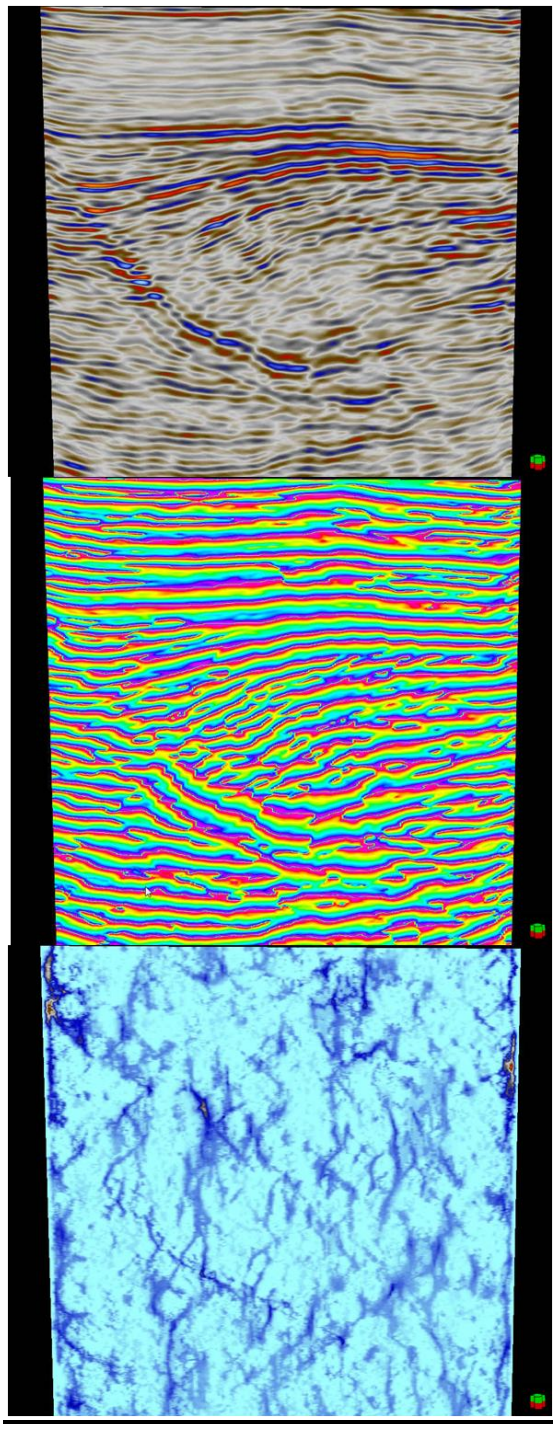

Figure 29. a) Original seismic, b) instantaneous phase, c) proposed workflow.

4.3 Application of composite attribute to Hitts Lake Field Data

The proposed workflow is applied to the Hitts Lake Field seismic dataset. The focus study area lies inside inlines 1001-1120 and crosslines 3003-3174. The interest area also lies between 500 and 3000 ms, where large normal faults generate grabens (Mexia-Talco Fault Zone), as discussed in chapter 1. Figure 30 shows a cross section of inline 1072, where we can clearly observe the graben.

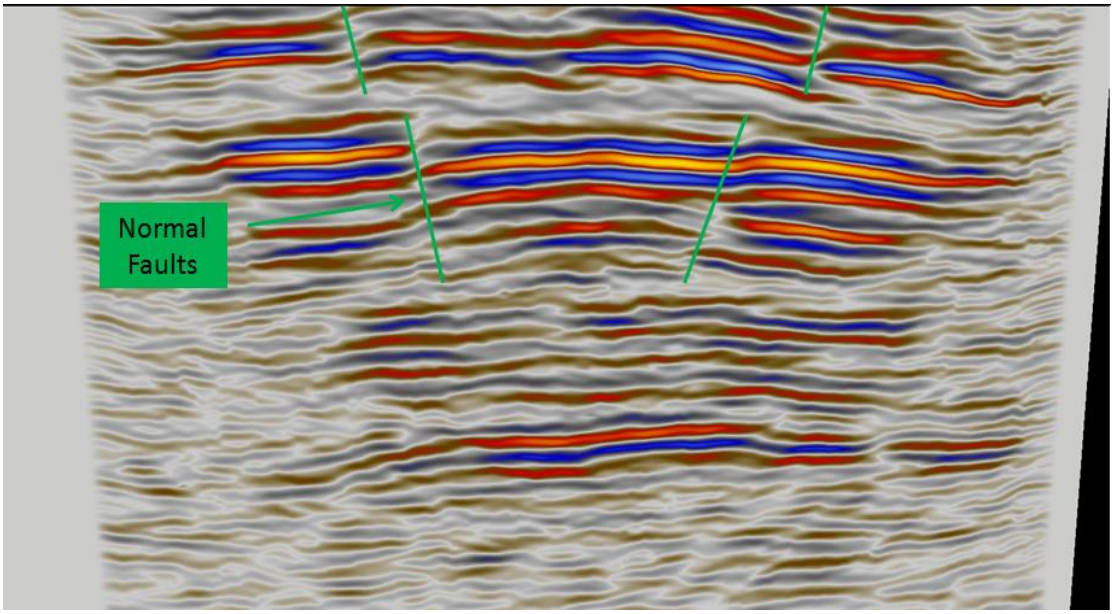

Figure 30. Inline 1072 showing normal faulting that forms a graben.

The objective of this project is to map all present faults. Based on this objective we inspect the amplitude spectrum of the data (observed in figure 31) and determine the frequencies to be used for the rest of the study. The frequency dependent amplitudes are then compared to determine if the chosen frequencies are the best characterizer of the geological features targeted to be mapped. The chosen frequencies are 35 and 40 Hz.

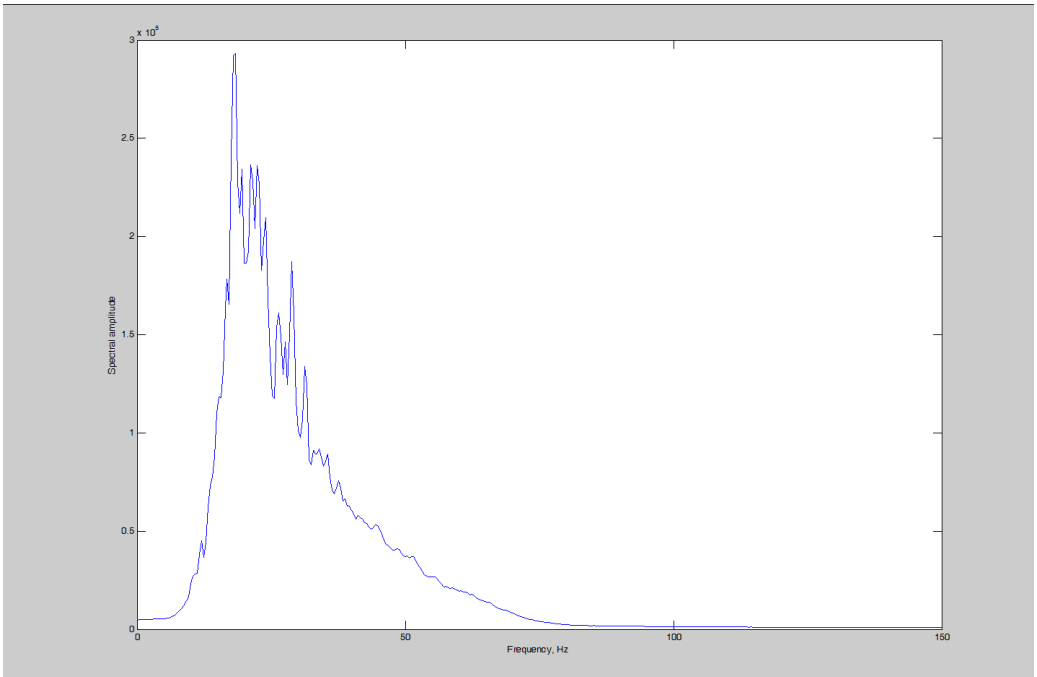

Figure 31. Average amplitude spectrum of seismic traces from the interest area.

4.3.1 Parameterization

Similar to the synthetic models, the preconditioning steps are mostly automatically parameterized. The frequencies used in the low pass bandpass are also [-100, -50, 5, 10] (in Hertz). The traces are averaged to their next 21 traces in both x and y directions.

Constrained Least Squared Spectral Analysis will be processed in Stratton Field seismic dataset using a 20 ms window.

We will calculate several edge enhancing attributes to the selected frequency dependant phase spectra. These include Coherence, Chaos, Variance, Most Positive Curvature, and the Laplacian Operator. The attributes are applied with a vertical window

of 9 samples and a lateral window of 3 samples. The data is sampled at 2 ms (therefore the vertical window is 18 ms long).

The next step will be to apply principal component analysis that will include the previously calculated attributes as inputs.

4.4 Results

The results and original data were loaded into Petrel once the workflow was completed. Figure 32 shows the seismic response, instantaneous phase response, and the workflow applied on inline 1072. More results, and the discussion of these, will be shown in the next chapter.

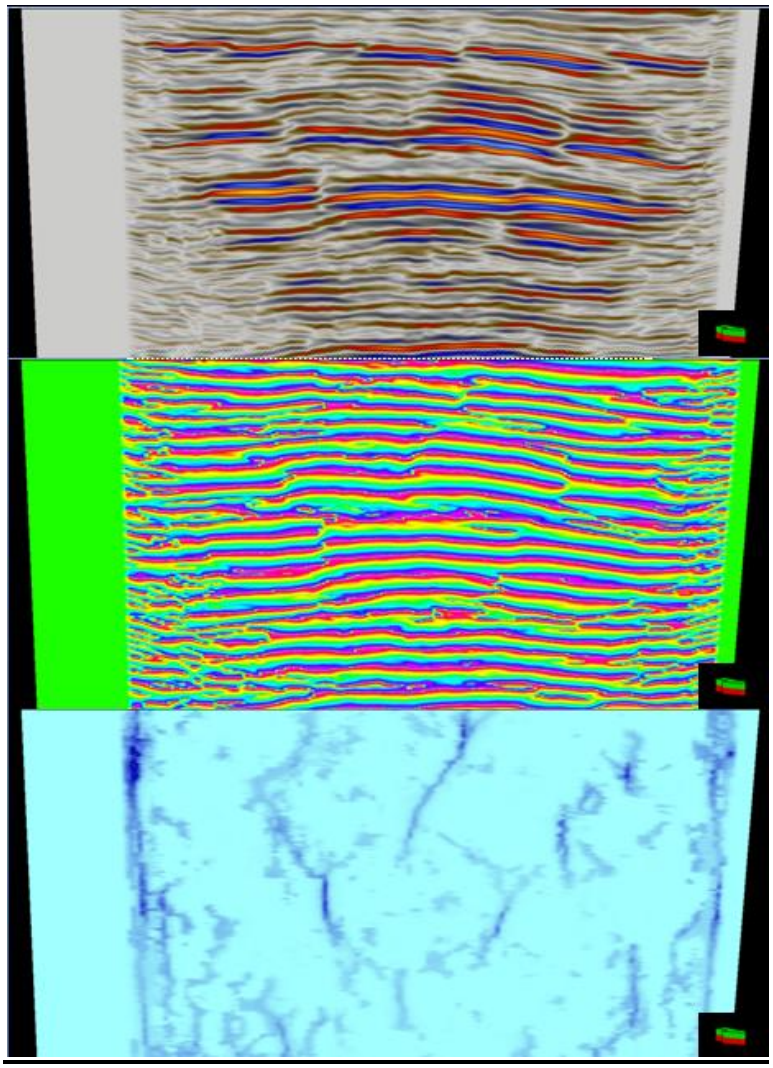

Figure 32. a) Original seismic, b) instantaneous phase, c) proposed workflow.

Chapter 5

Discussion of Results

5.1 Observations

Figure 33 displays the results for the proposed workflow in the Stratton Field data at time 2200 ms, which is observed in figures 34a, 34b, and 34c. This image serves to guide us with respect of the listric fault investigated, as the vertical displays are of inline 142, and time slices at 2200 ms.

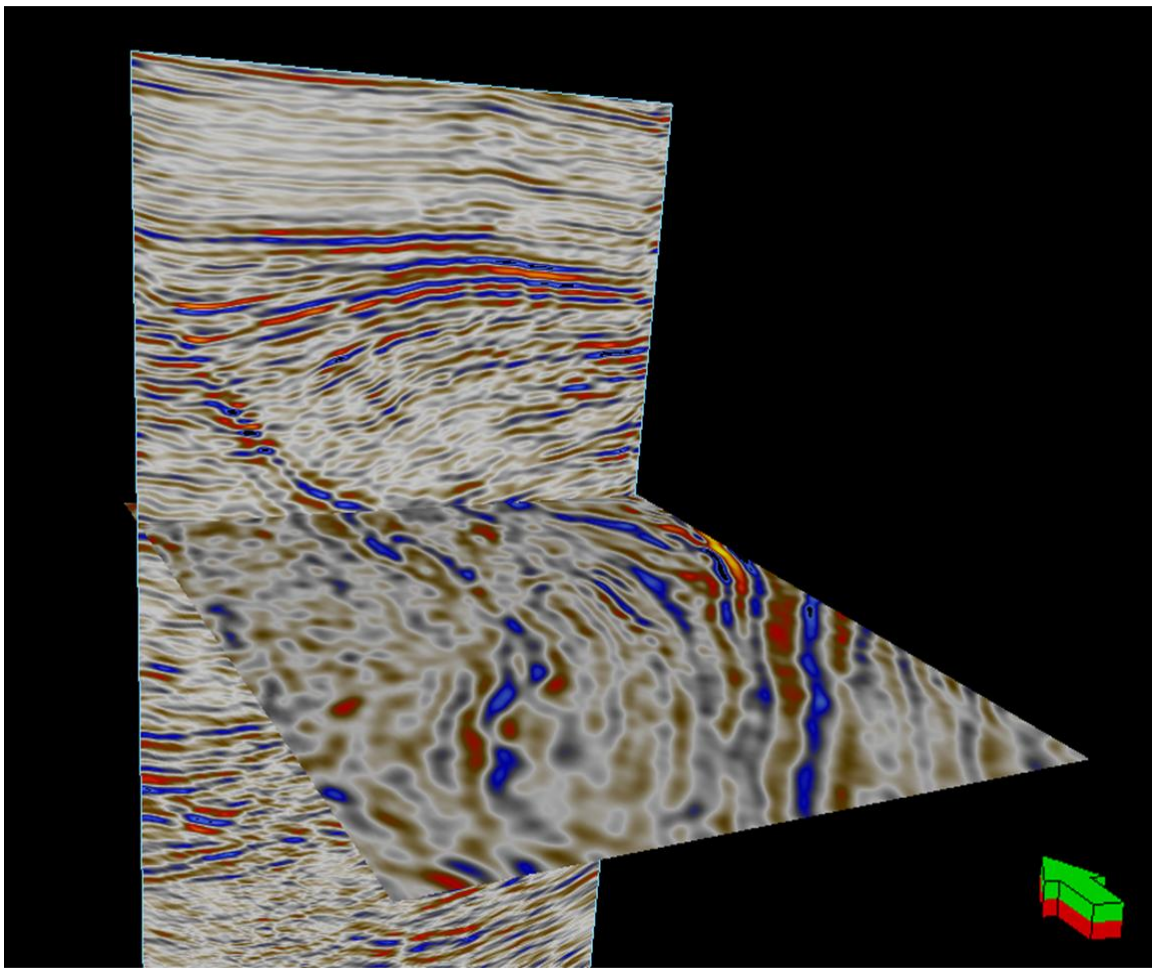

Figure 33. Cross-section of inline 142 as time slice 2200 ms cuts through it.

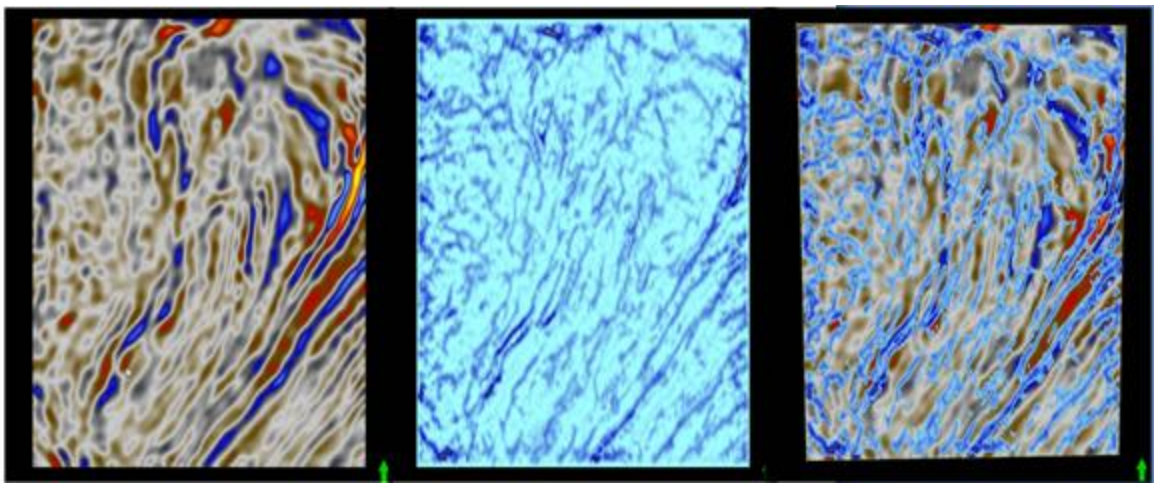

Figure 34. Time slice at 2200 ms a) extracted from seismic, b) extracted from the composite attribute, c) overlay of composite attribute over original seismic.

Excellent correlation is observed between the final results and the original seismic. All faults appear to be detected by applying this methodology.

Similar results can be observed in cross-sectional view, as displayed in figures 35a, 35b, and 35c. These cross-sectional panels are approximately 900 ms long.

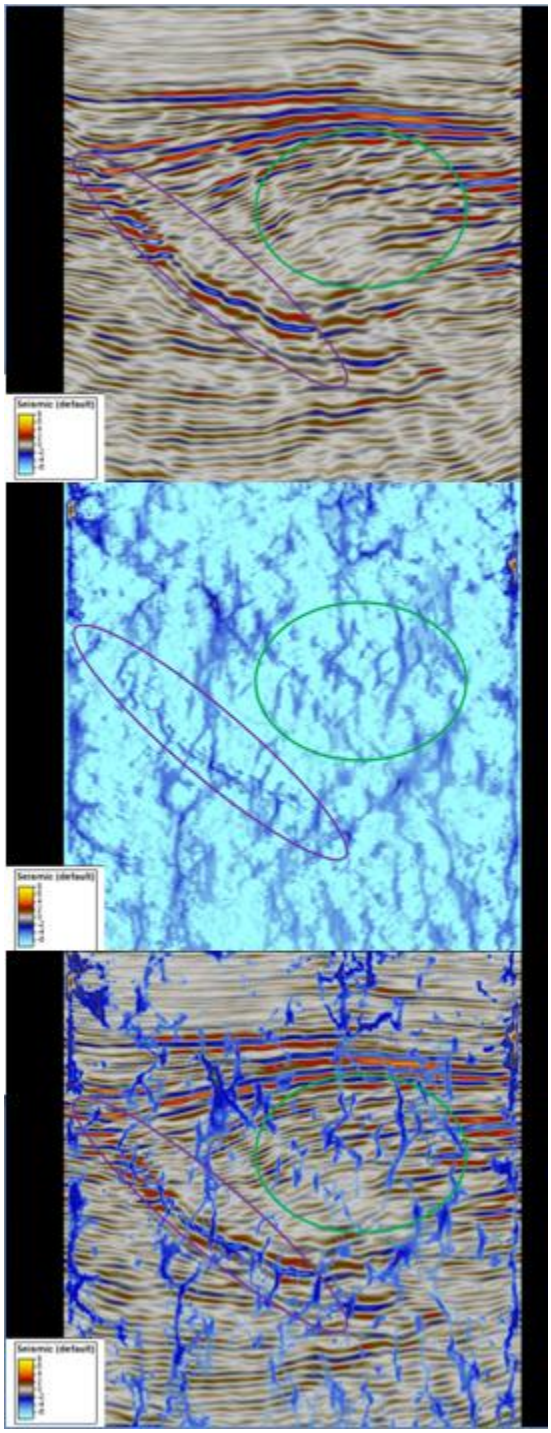

Figure 35. Inline 142 a) original seismic input, b) composite attribute, c) overlay of composite attribute over original seismic.

This result shows how well the attribute operates. Several faults are detected with high level of precision and detail. The purple oval shows how the composite attribute detects the listric fault. This will be important later as we will observe the responses for the commonly used attributes in the industry for the same event.

The green oval shows a fairly chaotic area where we can observe smaller antithetic faults that compartmentalize the on lapping sand. These sand compartments become important reservoirs in the area. The composite attribute clearly shows the response of faulting in the area, which would be of great importance when deciding where to locate future prospects. The green oval will also be observed in the commonly used attributes.

Figure 36 serves to guide us with respect to the graben investigated. The vertical display shows inline 1072 and the horizontal display shows time slice 1486 ms.

Figure 37 displays the result for the composite attribute in the Hitts Field Lake data at time 1486 ms, which are observed in figures 37a, 37b, and 37c.

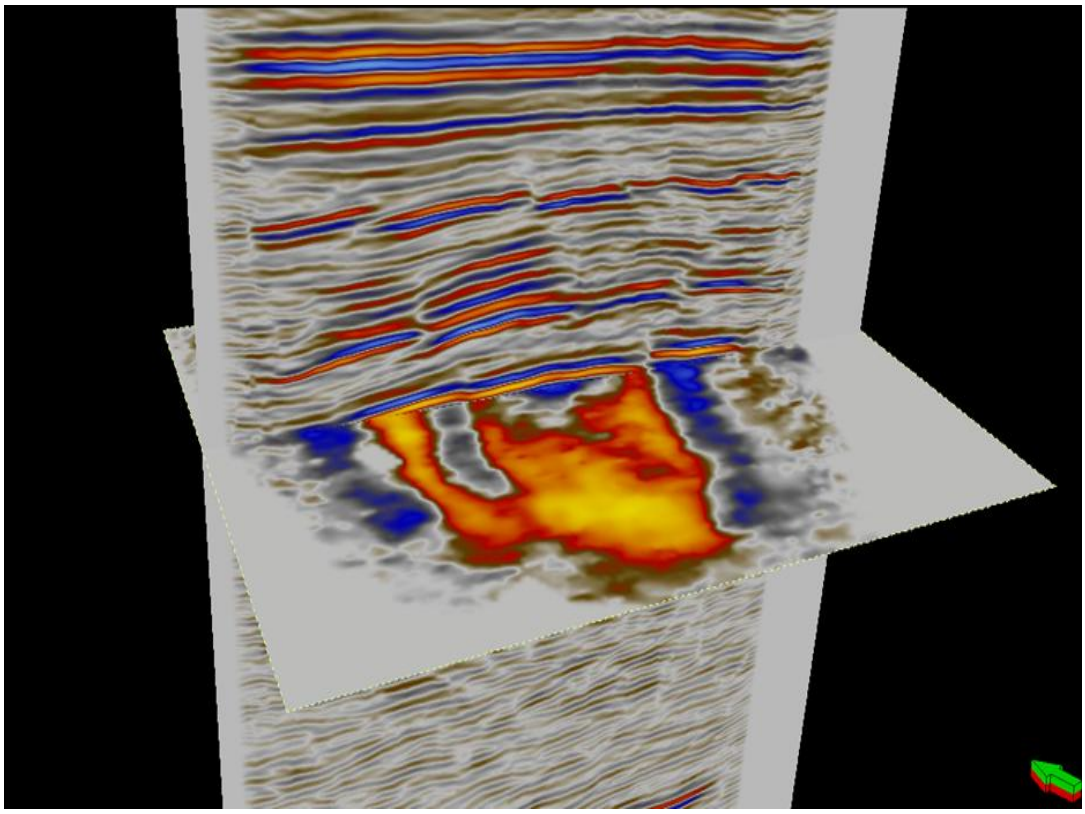

Figure 36. Cross-section of inline 1072 as time slice 1486 ms cuts through it.

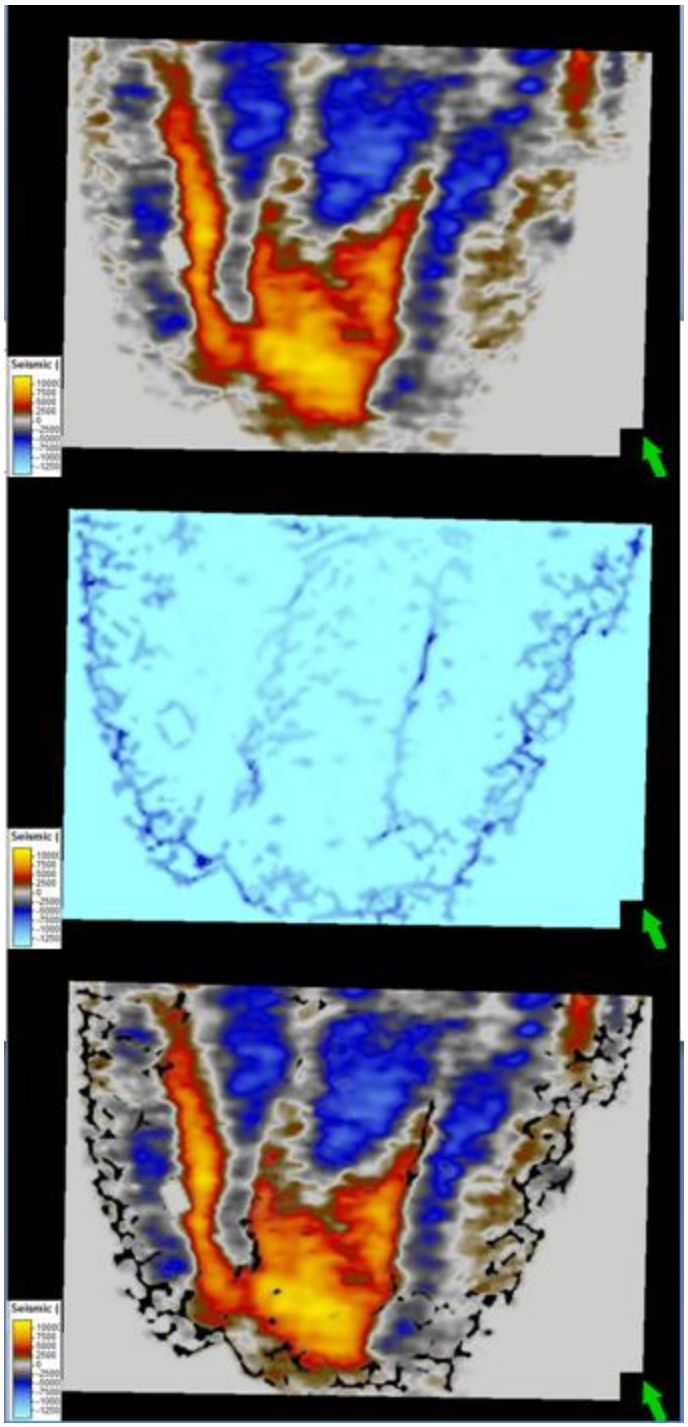

Figure 37. Time slice 1486 ms, a) extracted from seismic, b) extracted from composite attribute, c) overlay of composite attribute over original seismic.

The results observed are excellent. The main faults are clearly detected by the attribute. It is important to note that the overlay image is limited by the level of opacity that can be applied to clean the background. In this case, the process of removing the background for the overlay also removed some of the faults that in base map do not appear obvious, but are clearly observed in the attribute's base map. Similar results are observed in vertical cross-section (figure 38).

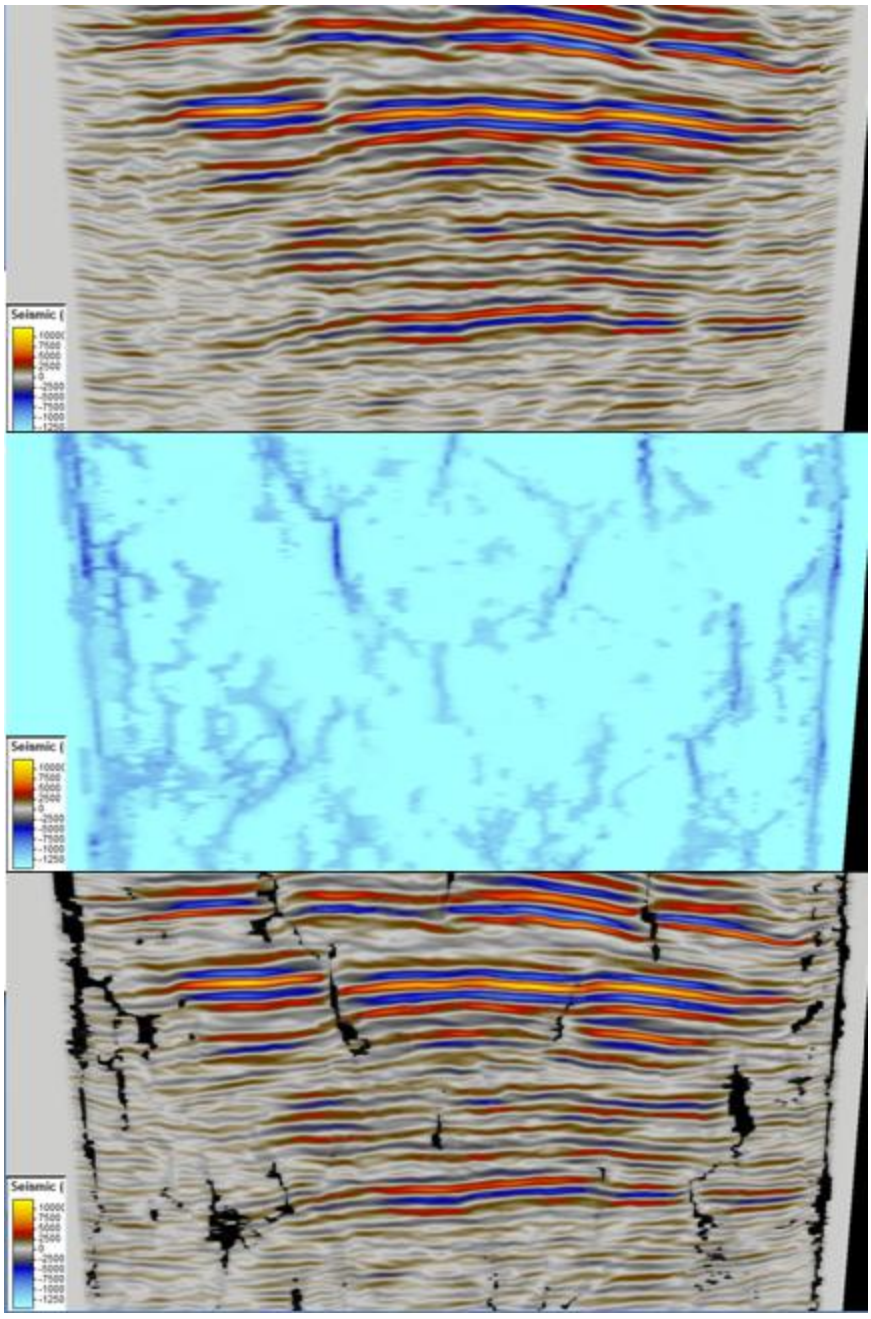

Figure 38. Inline 1072, a) Original seismic input, b) composite attribute, c) overly of composite attribute over original seismic.

Vertical displays show how the attribute detects the normal faults that build the graben (which is the objective of the project) as well as other faults observed in the area. The lateral extent of these faults is observed in base map (figure 37) which allows the user of the attribute to simply map the fault plane of the faults that encompass the graben, as well as the lateral extent of this structural feature.

5.2 Comparison between Proposed Workflow and Industry Standards

The previously observed results show the composite attribute when compared to the seismic section. We will now observe how it compares to some of the most commonly used attributes in the industry; in this case, coherence and most positive curvature.

Figures 39a and 39b show coherence and most positive curvature (respectively) in time slice, at 2200 ms. Figures 39c and 39d show the composite attribute overlaying the previous images. This example corresponds to the Stratton Field dataset.

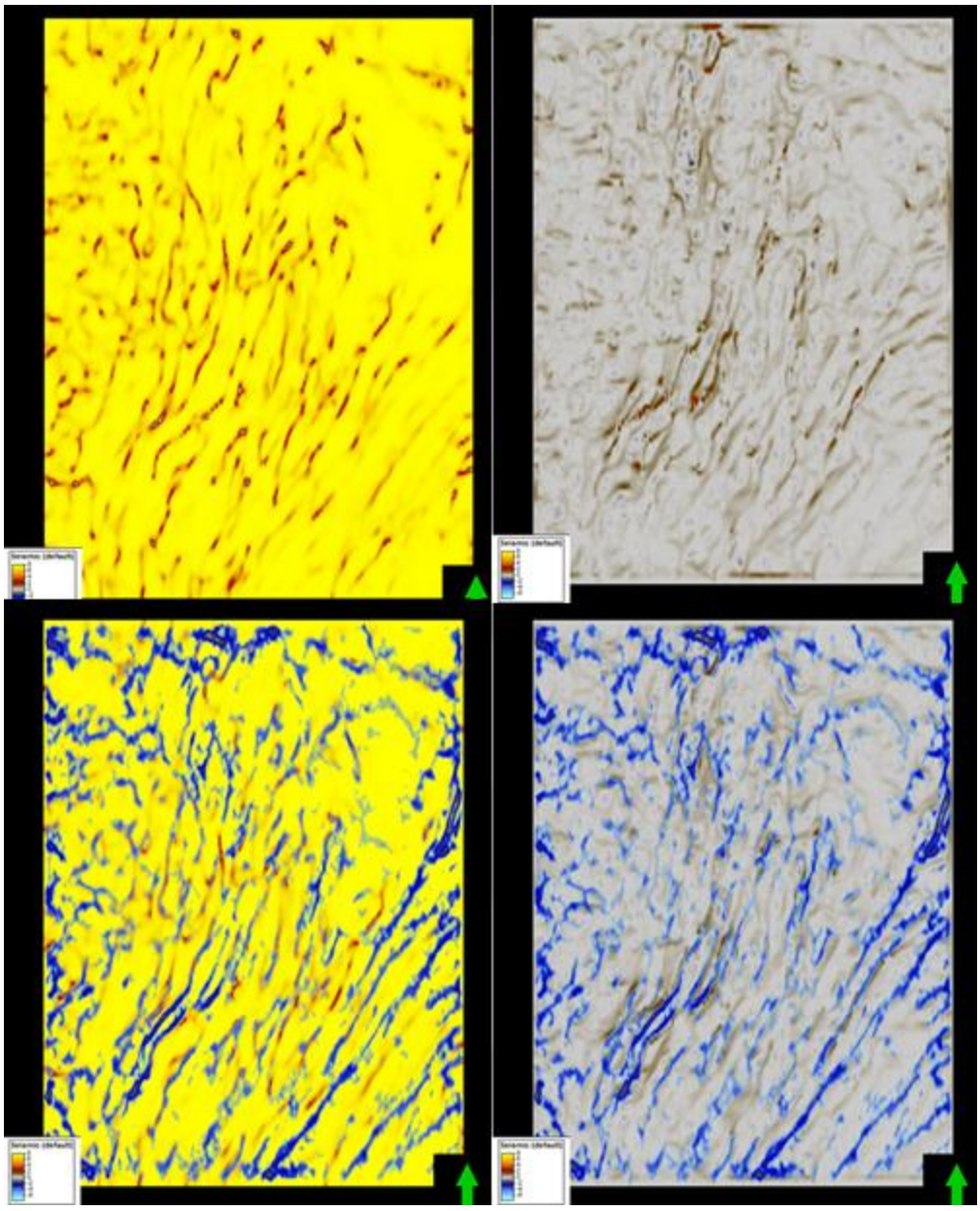

Figure 39. Time slice at 2000 ms, a) extracted from coherence, b) extracted from most positive curvature, c) composite attribute over coherence, and d) composite attribute over most positive curvature.

When comparing figures 34 to 37 we can observe that while both coherence and most positive curvature perform positively, the proposed workflow shows superior results. Both coherence and most positive curvature detect the largest, regional faults; but fail to detect fault in dipping environments (towards the south-eastern area of the time slice). It is also noticeable that the proposed attribute shows better connectivity as well as a better fault character.

The difference between the attributes is most noticeable in cross section. Figures 40a-d show coherence and most positive curvature extracted on inline 142. They also show the composite attribute overlaying the previous.

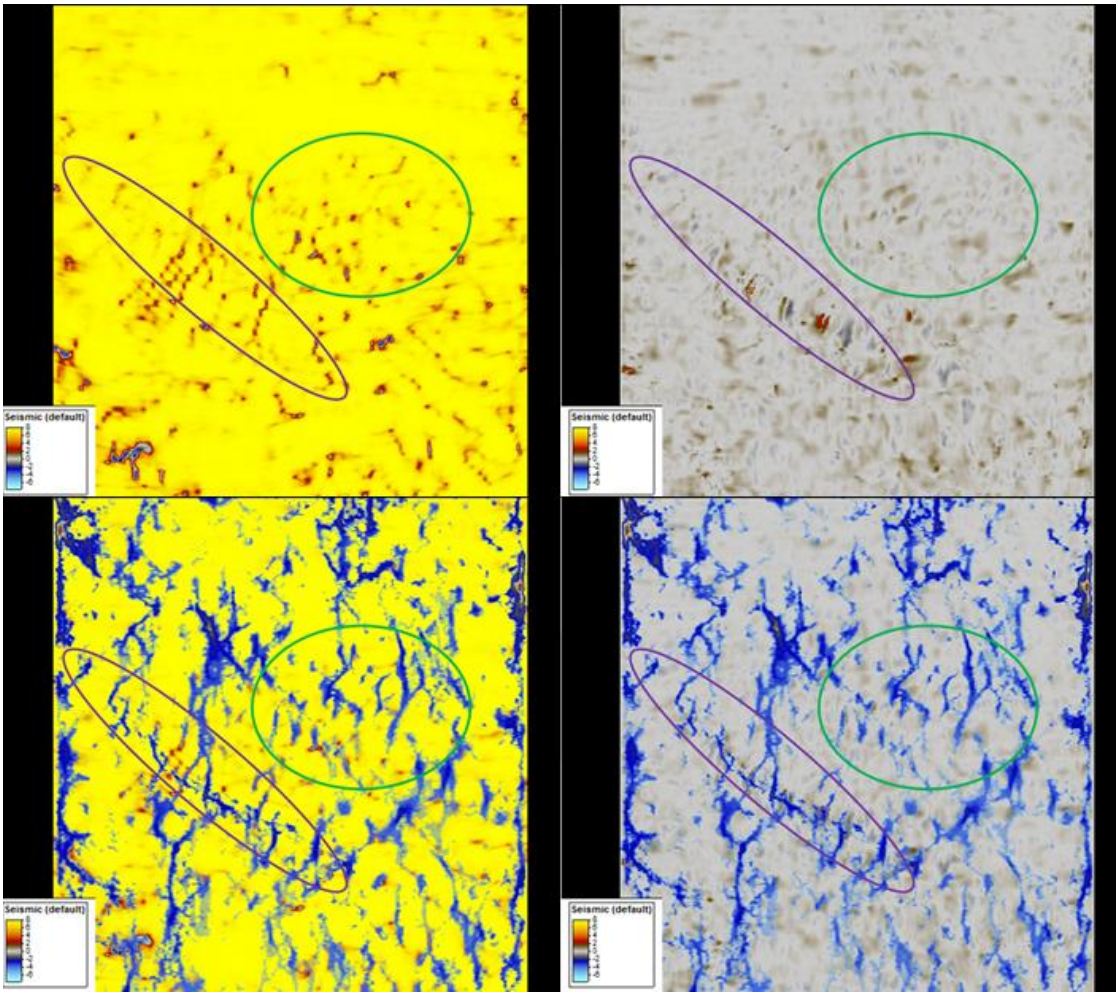

Figure 40. Inline 142, a) coherence, b) most positive curvature, c) composite attribute over coherence, and d) composite attribute over most positive curvature.

Figure 40 shows better fault connectivity and extension, as well as detection. The purple oval shows how coherence does not pick the listric fault, and most positive curvature appears like it does, but it is not well characterized. The composite attribute shows the best result in this aspect.

The green oval shows the compartmentalized area. The response in both attributes is poor; and as they approach the bright reflectors, the response worsens. The composite attribute shows better fault characterization in this area, and it is not affected by the

brightness of the amplitudes of the seismic data (this is because the attribute is based on the phase spectra). Fault connectivity in this attribute shows how the separate compartments are divided, which is very important when designing the drilling plan.

Figures 41a-d show coherence and most positive curvature at time slice 1486 ms. They also show the composite attribute overlaying them. This next example corresponds to the Hitts Lake Field Data.

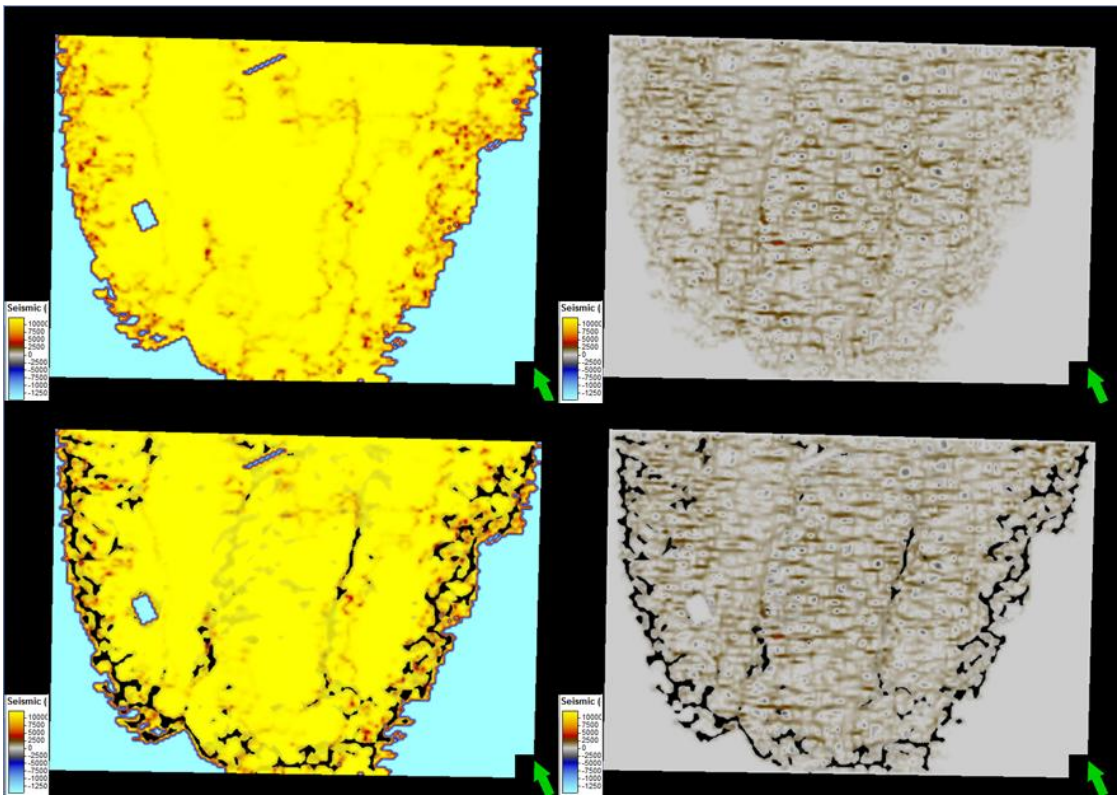

Figure 41. Time slice 1486 ms, a) coherence, b) most positive curvature, c) composite attribute over coherence, and d) composite attribute over most positive curvature.

The north eastern 2 main faults observed in the base maps (that form the graben) are mapped to their complete lateral extent by the composite attribute. The coherence attribute detects the faults well but it loses the western most one. Most positive curvature detects these two faults on their entirety, but appears to be affected by parallel responses which are probably related to acquisition footprint. The composite attribute detects both faults to their complete lateral extent and at the same time discriminates signal from acquisition footprint. This image also shows the overlay problem observed in figure 41.

Vertical cross-sections comparing both attributes to the composite attribute are presented in figures 42a-d. These figures correspond to inline 1072.

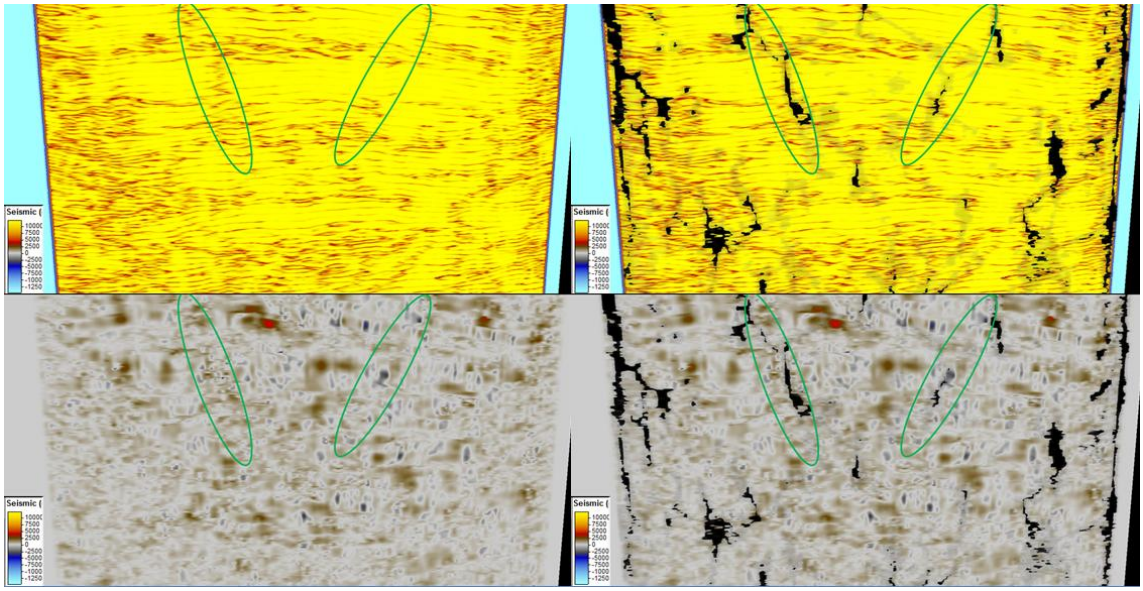

Figure 42. Inline 1072, a) coherence, b) composite attribute over coherence, c) most positive curvature, d) composite attribute over most positive curvature.

The cross-sections show the effectiveness of the attribute. It detects the faults observed in the area. When compared to both coherence and most positive curvature, it can be noted that coherence also detects the faults (green ovals) but it also highlights non-dipping events which are not real seismic discontinuities. These are omitted by the

composite attribute. The right most fault related to the graben is not detected by coherence (right green oval) but it is detected by the attribute.

5.3 Validation of Results

Two different techniques are used in order to validate results. The first is co-rendering the seismic volume with the composite attribute volume. The second is interpreting faults in the well logs and matching the well log interpretation to the fault detection volume.

5.3.1 Co-rendering

The first volume co-rendering shows the seismic progression from inline 142 to inline 117, at 5 inlines intervals; this is contrasted with a static time slice of the composite attribute at time 2200 ms. Figure 43 shows how the major faults (including the listric fault) are detected by the attribute. Figure 44 shows the same progression with the composite attribute instead of the original seismic. It can be determined how the attribute also detects the new major faults towards the north east part of the section, which further compartmentalize the on-lapping sand.

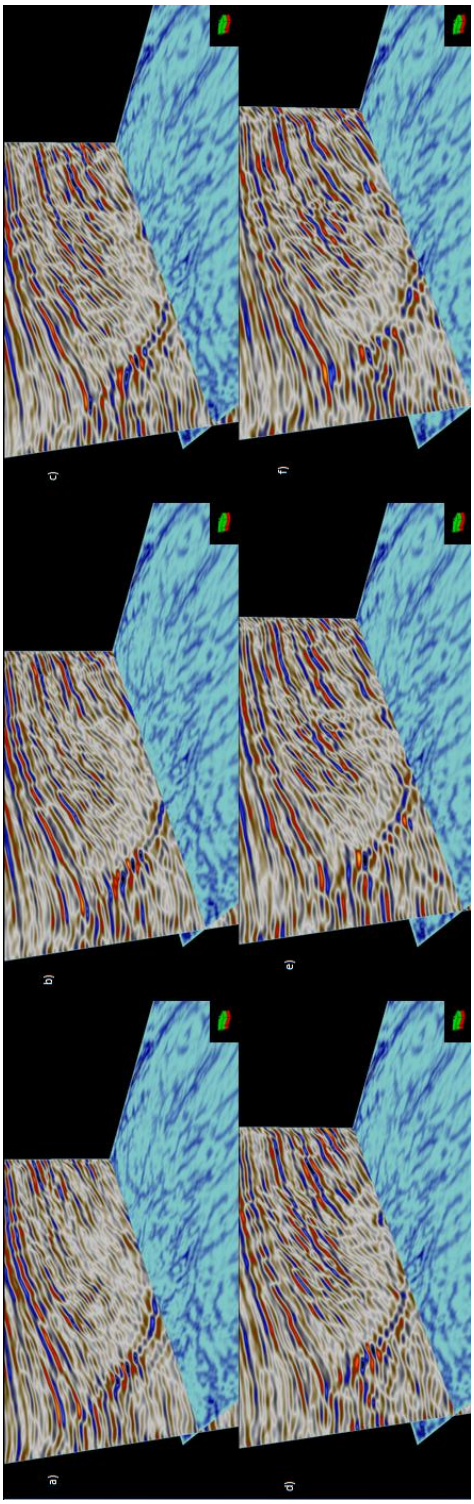

Figure 43. Co-rendering of seismic (inlines) vs. composite attribute (time slices).

From a) to f) goes from inline 142 to 117, in intervals of 5 inlines.

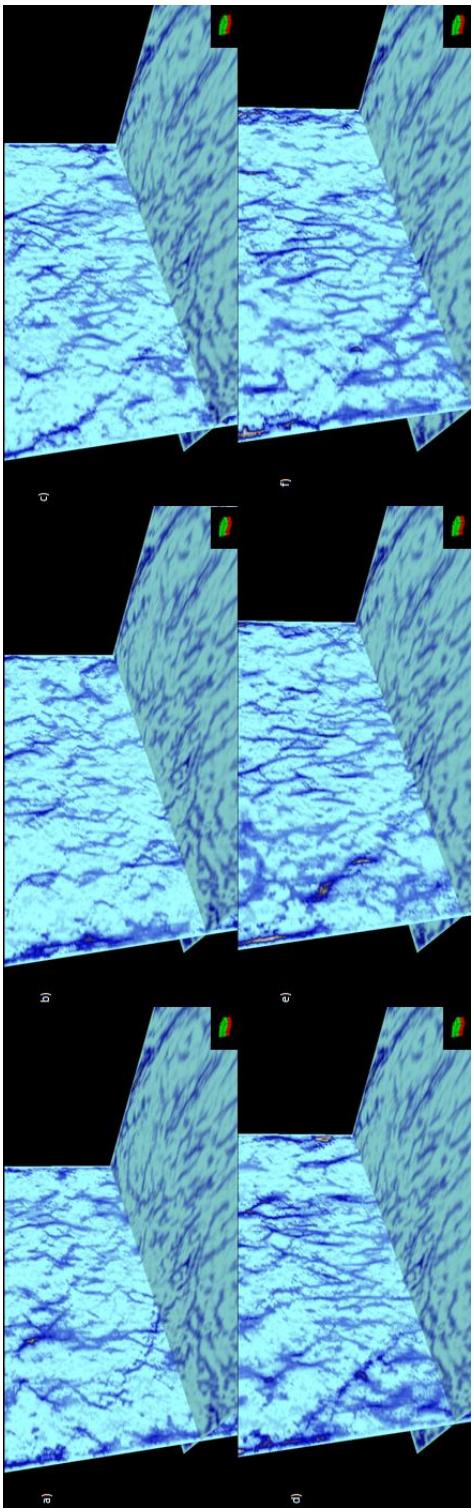

Figure 44. Co-rendering of composite attribute (inlines) vs. composite attribute (time slices).

From a) to f) goes from inline 142 to 117, in intervals of 5 inlines.

5.3.2 Well Log Analysis

Location of faults can be determined in wells by correlating different wells to each other. Correlation of packages with the same signature in different logs represents the same formation and faults are observed in wells when these packages either repeat or are missing.

The location of these faults in the well are called fault cuts and the interpretation of these is important because they allow us find faults that might be below seismic resolution.

Figure 45 presents a base map showing the area of the Hitts Lake Field, as well as the direction of a cross section across wells perpendicular to the direction of the fault.

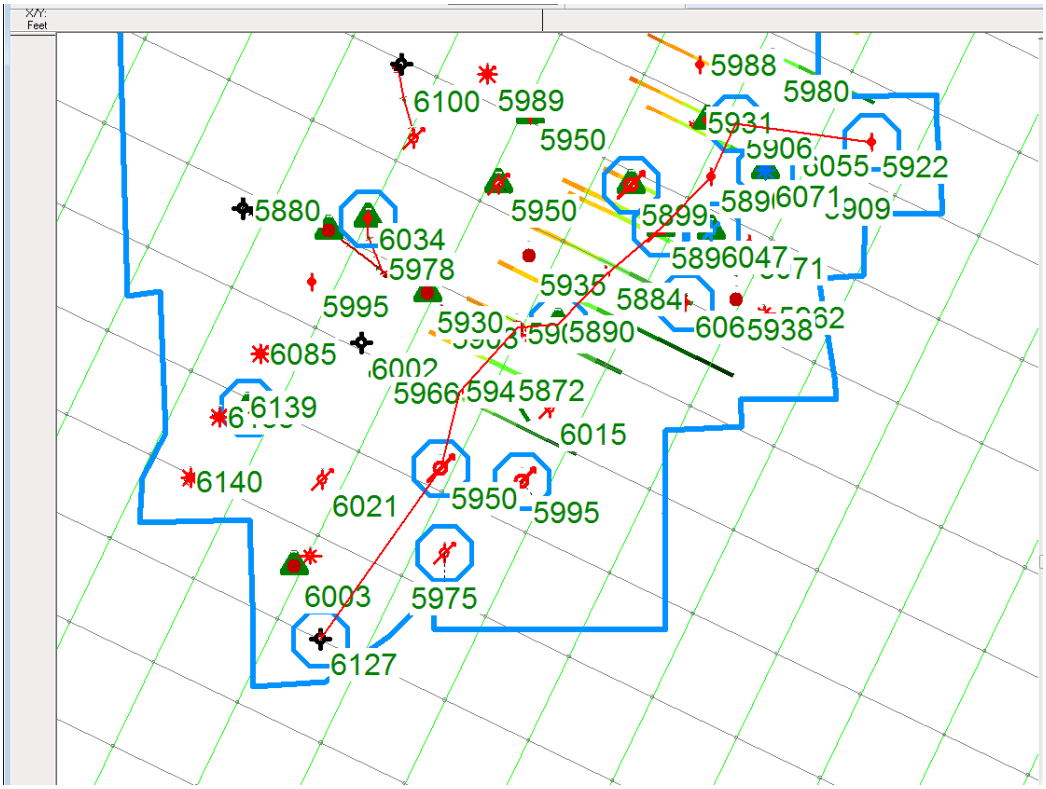

Figure 45. Base Map of Hitts Lake Field.

Figure 46 shows the cross section. The formations are correlated based on their SP and Resistivity logs.

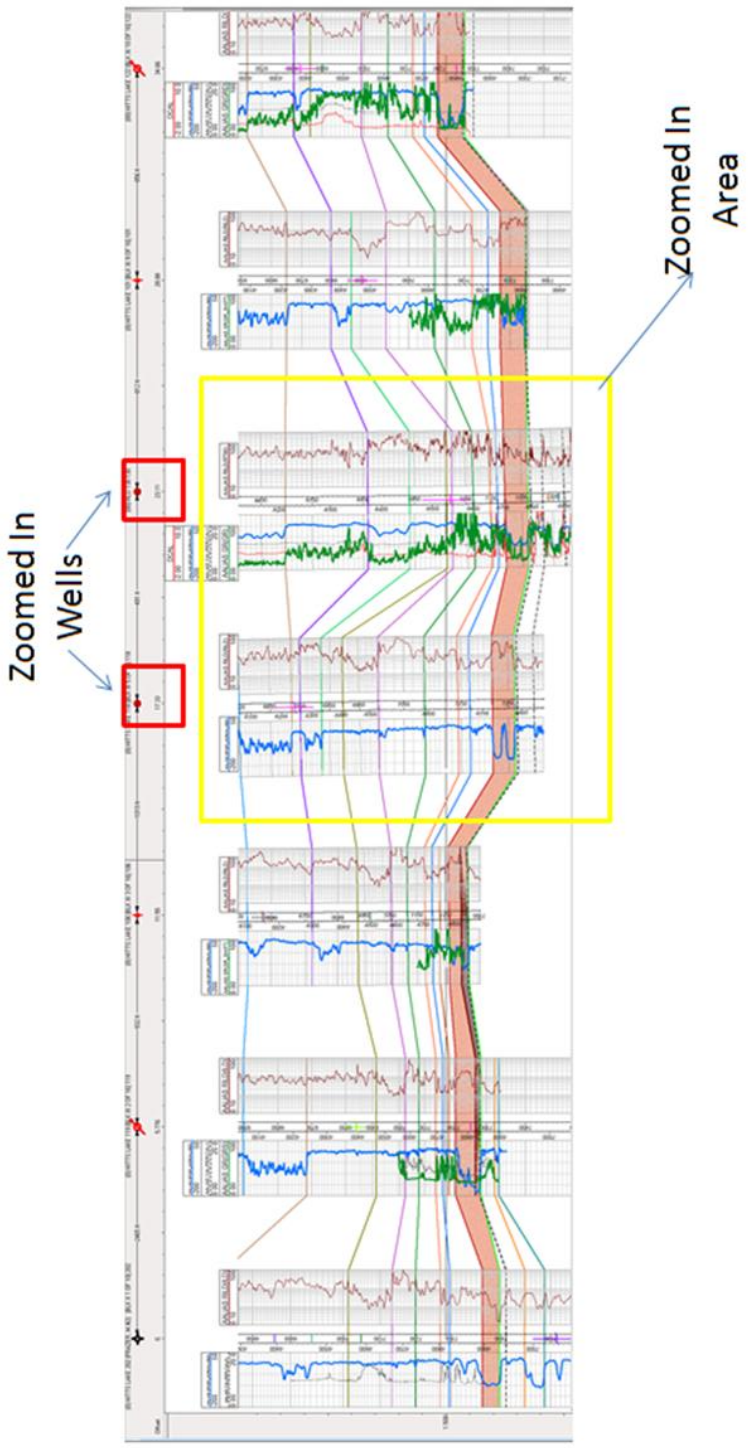

Figure 46. Cross section of the Hitts Lake Field.

Figure 47 shows a zoomed in section of the previous cross section. This zoomed in section includes wells Hitts Lake 118 and HLU 130. Two fault cuts are observed in these wells. The correlations of common events are done using the SP and resistivity logs. Once this events are correlated, two events are observable on the well HLU 130; the repeated section (with respect to the well Hitts Lake 118) at the top of the well, and the missing section at the bottom of it. These exhibit the presence of faults in the wells.

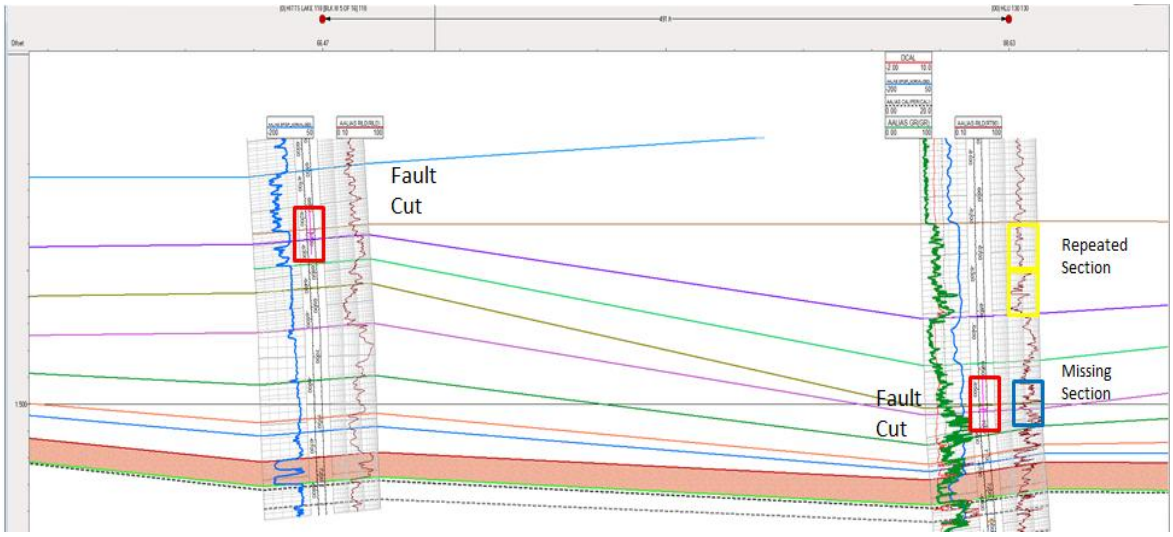

Figure 47. Cross section between wells Hitts Lake 118 and HLU 130. Missing and repeated sections are observed and fault cuts are located.

The interpreted fault from fault cuts over the seismic and composite attribute are shown in figures 48a and 48b. Figures 49a and 49b show the same images without the wells over the seismic to more clearly observe the interpreted fault over the attribute.

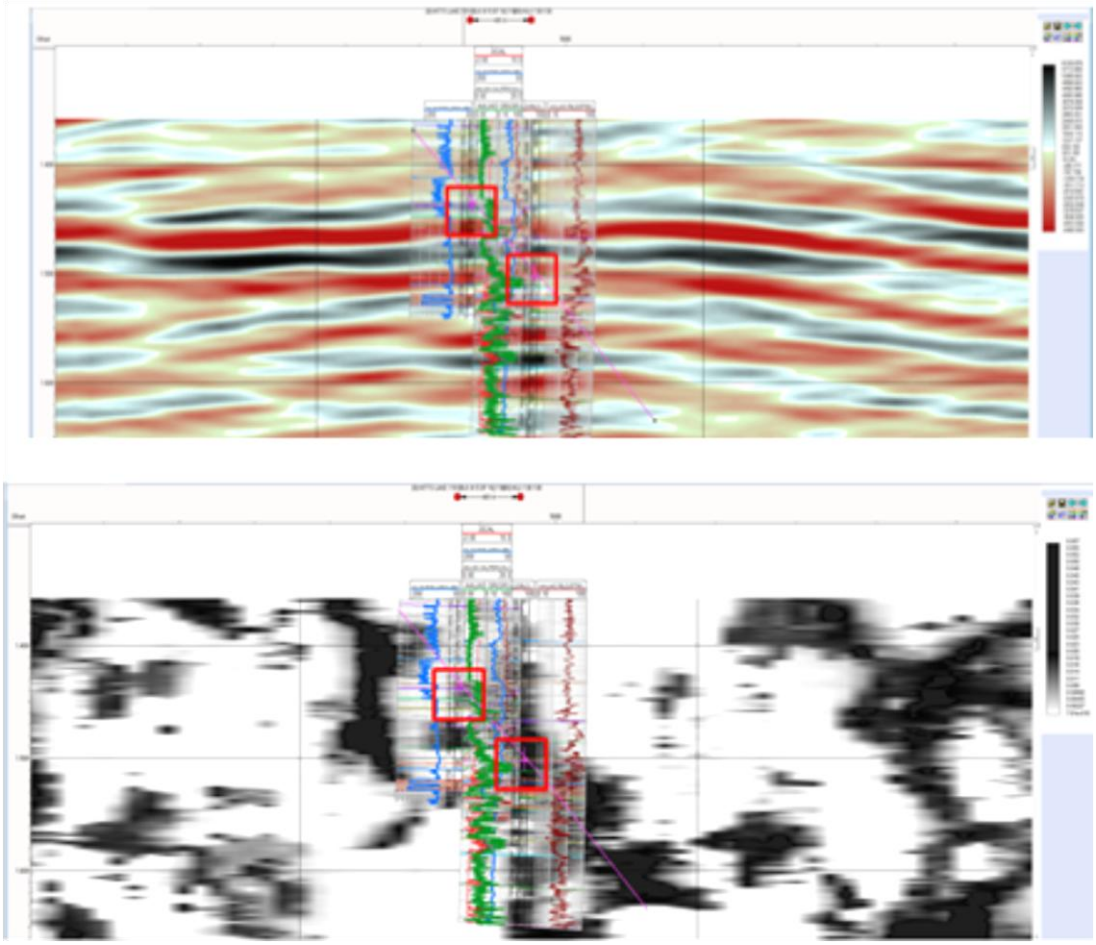

Figure 48. Interpreted fault over a) seismic and b) composite attribute.

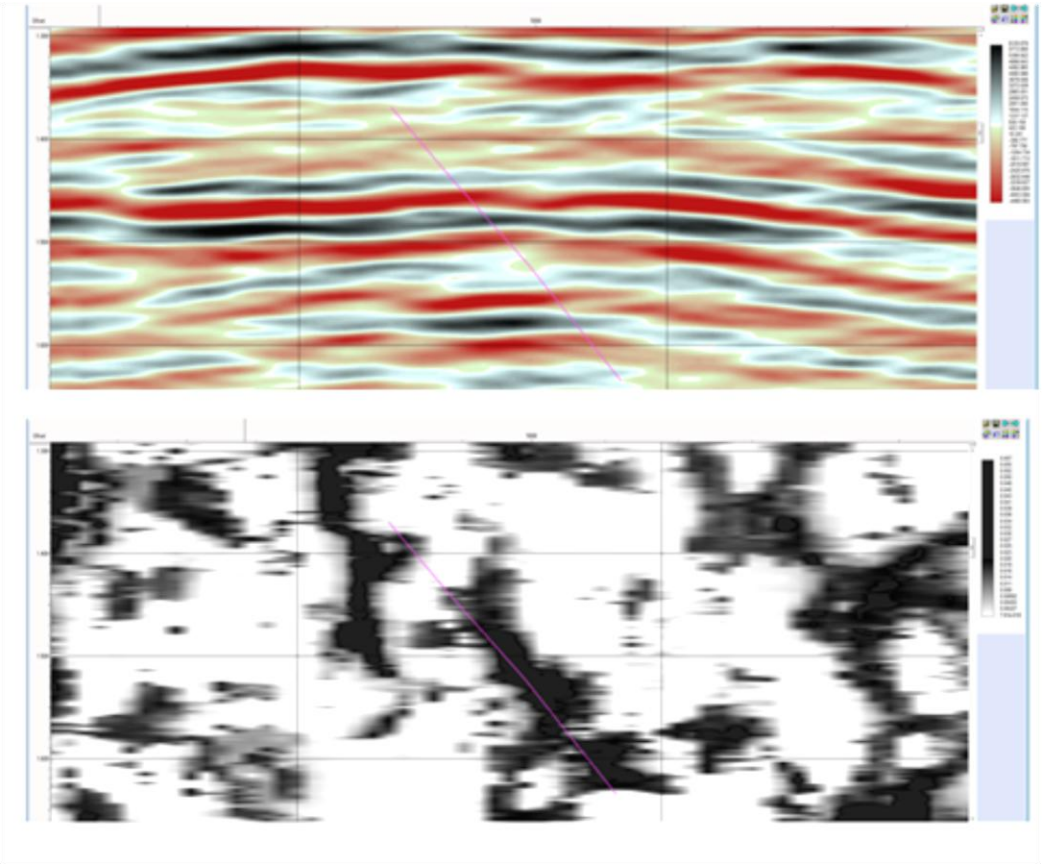

Figure 49. Interpreted fault over a) seismic and b) composite attribute (wells not shown).

It can be observed that the interpreted fault, which appears to be below seismic resolution but observed in the well, is detected by the composite attribute. This is possible by the response of select frequencies.

5.4 Fault Density and Orientation Analysis

An advantage of producing an effective 3-dimensional fault attribute is that it allows the user to study fault density and orientation relationships. This is useful information when characterizing a reservoir in which faulting can have a significant impact. At the same time, studying fault orientation variations can allow the user some insight regarding the fracture system present in the area.

Figures 50a-d show fault density and orientation of the studied area in the Stratton Field, as well as the composite attribute overlaid over them.

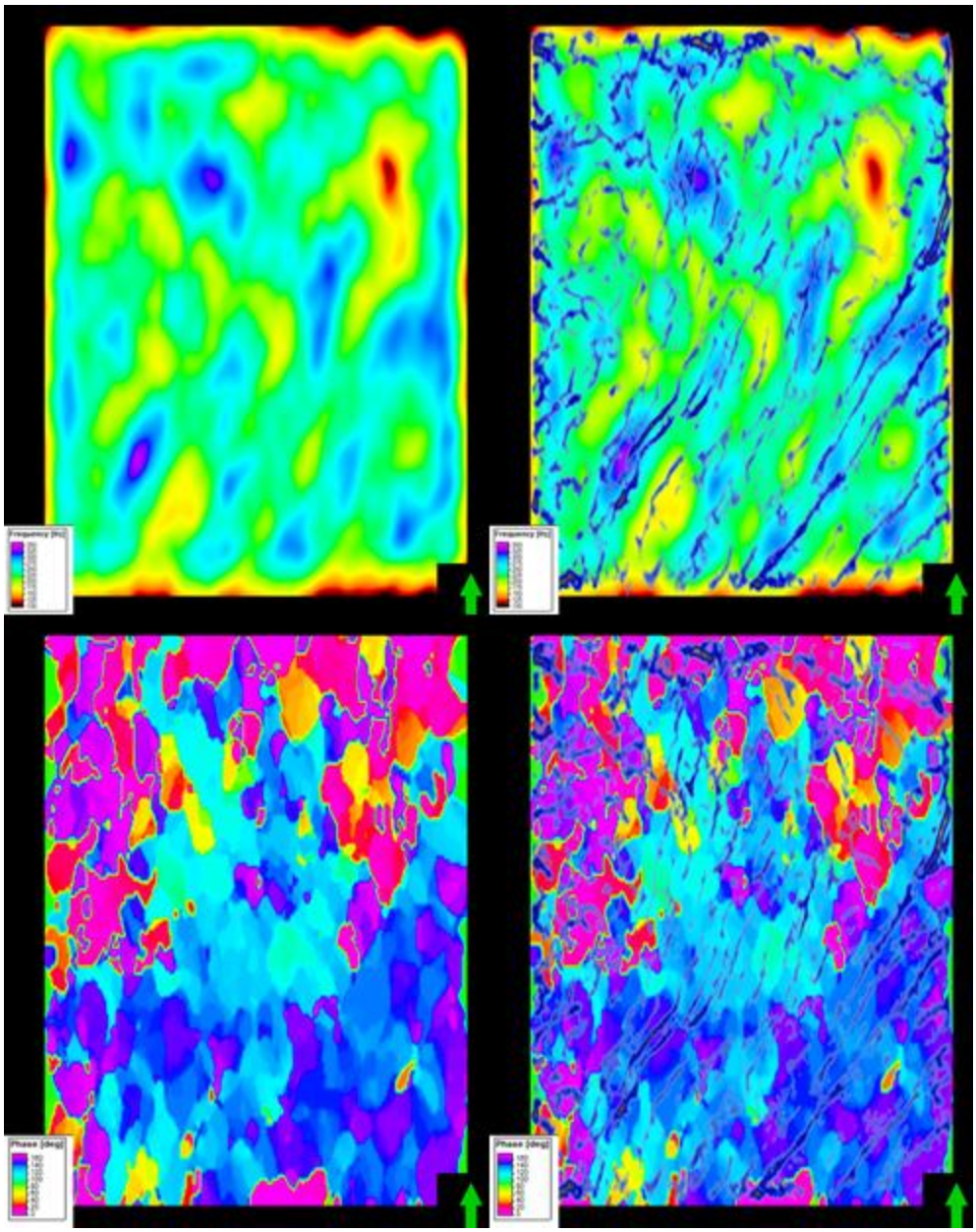

Figure 50. Time slice at 2200 ms showing a) fault density, b) composite attribute over fault density, c) fault orientation, and d) composite attribute over fault orientation.

Areas of high fault density present several faults. Similarly, the general direction of the faults goes from SW to NE, which is the main orientation observed in the fault orientation time slice. It can be noted that fault density corresponds to the information observed by the attribute.

Figures 51a-c show the composite attribute with rose diagrams. The rose diagrams are computed within the circle shown.

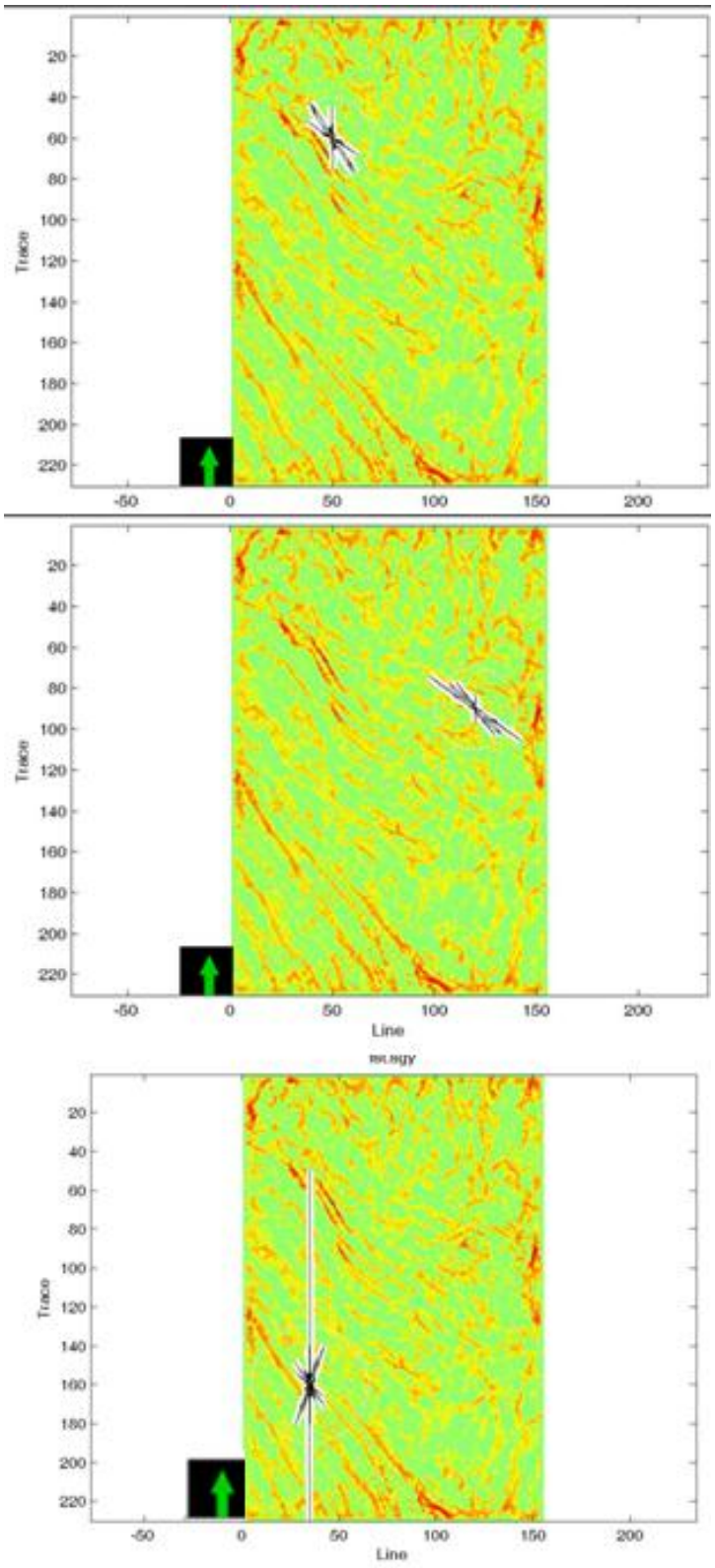

Figure 51. Time slice at 2200 ms showing rose diagrams on the composite attribute.

Figure 51a shows agreement between the orientation of the rose diagram and the fault's orientation. Similarly in figure 51b.

Figure 51c shows a major spike in the N-S direction which could be an artifact generated by acquisition footprint. The next principal orientation is close to perpendicular to the orientation of main faulting in the area, which is an indication of possible fracturing.

Figures 52a-d show fault density and orientation of the studied area in the Hitts Lake Field. They also show the composite attribute overlaying them.

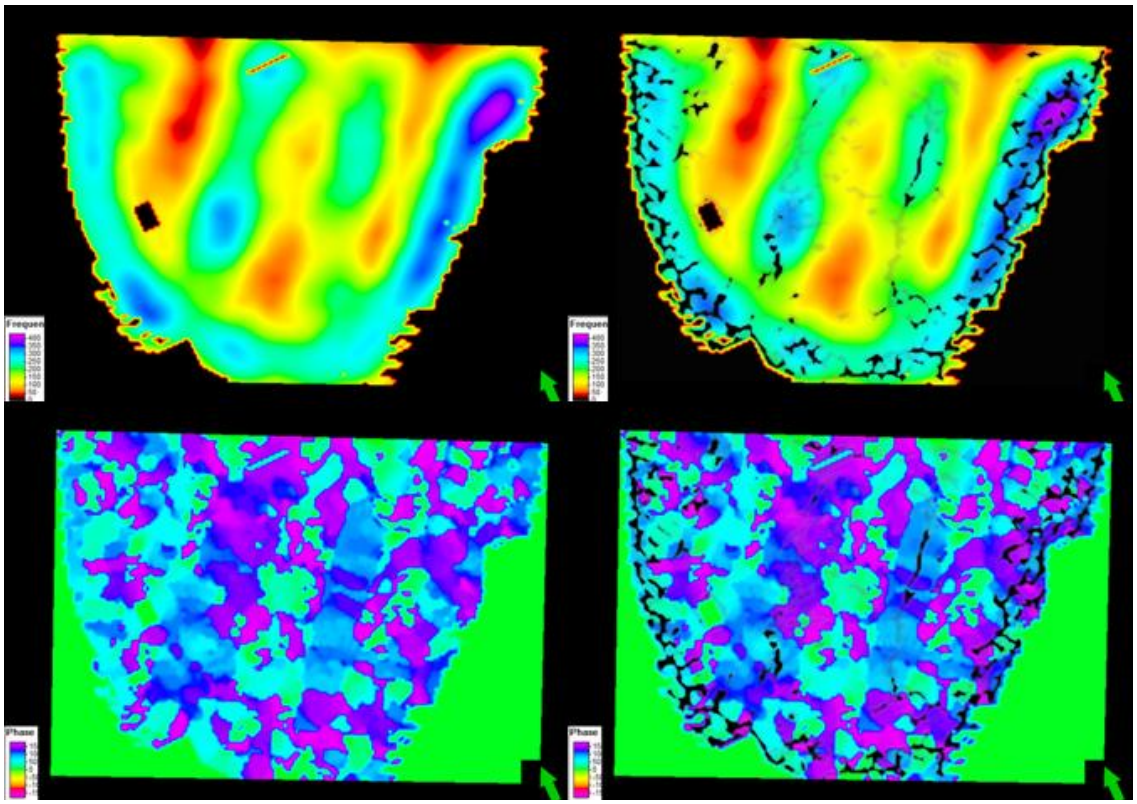

Figure 52. Time slice at 1486 ms showing a) fault density, b) composite attribute over fault density, c) fault orientation, and d) composite attribute over fault orientation.

It can be observed that the areas with higher fault density are those with the main NE-SW oriented faults. This response is also observed at the edge of the area of the survey with data. Where the data end, there is a discontinuity which is detected by the attribute as faulting.

Figures 53a-c show the composite attribute with rose diagrams. The rose diagrams are computed within the circle shown.

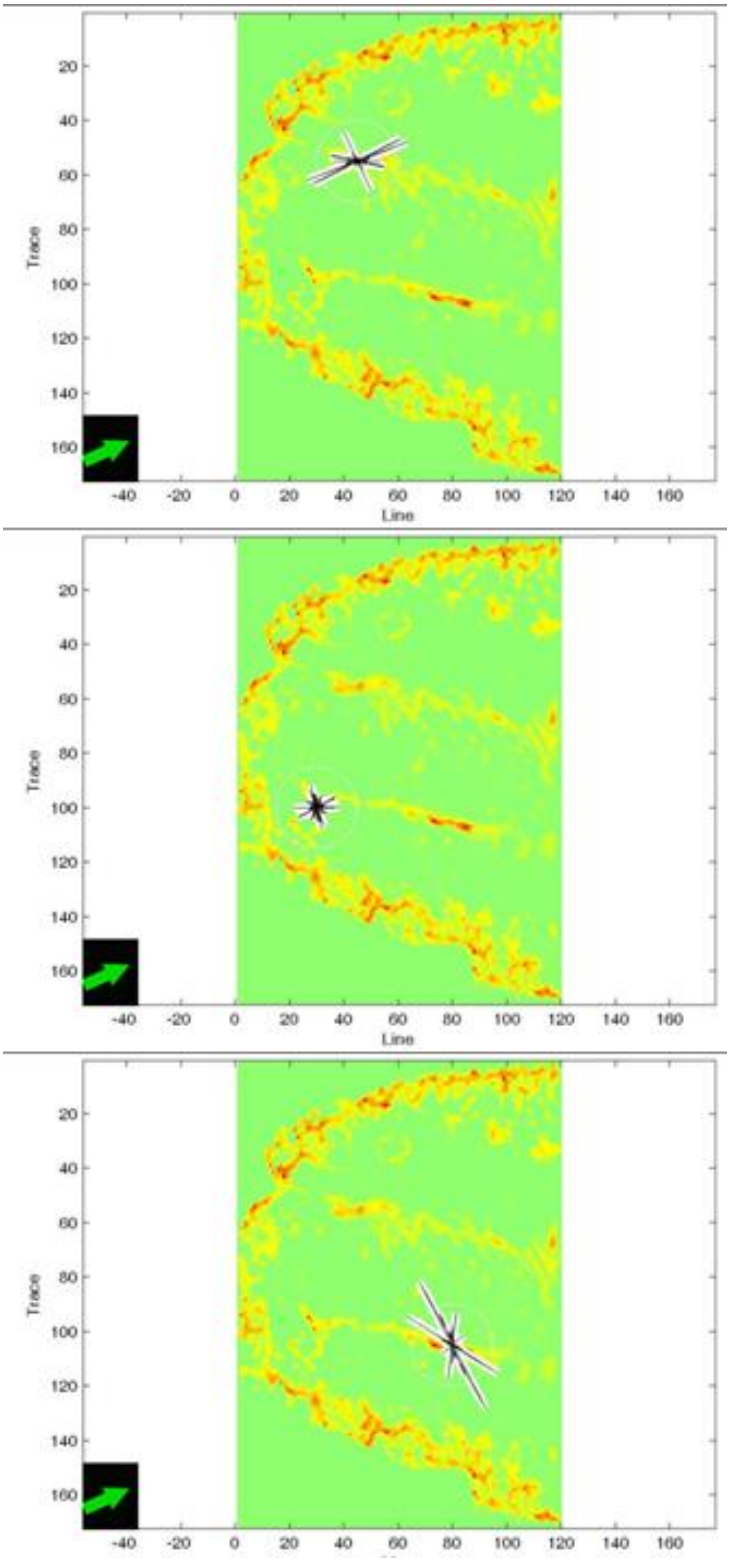

Figure 53. Time slice at 1486 ms showing rose diagrams.

Figure 53a shows the main fault orientation coincides with the rose diagram, highlighting the direction of the principal stress within the calculated area. It doesn't follow the direction of the main fault because the rose diagram is centered where there is a slight change of fault direction.

Figure 53b shows less variation in the amplitude of the rose diagram, indicating a chaotic area of stress (potential fracturing).

Figure 53c clearly shows that the main fault direction varies with the main direction of the rose diagram, which is an indication of fracturing (the average of all the fault angles within the area differs in orientation with respect to the main fault orientation).

5.5 Conclusions

The primary objective of these projects is achieved. We are able to characterize the listric fault for Stratton Field and the graben for Hitts Lake Field. Both major features are clearly detected by the composite attribute in the complete seismic section. Another important point was to observe how the attribute behaves with respect to other attributes.

The composite attribute showed excellent results when compared to other commonly used attributes for the same purpose. It has better fault connectivity and character than coherence and curvature appear to show. This is clearly observed in vertical section.

The validation process was successful. The attribute detects faults observed at well logging scale with precision and the co-rendering process shows that fault planes are not lost as we move laterally in the composite attribute volume.

Finally, the composite attribute allows us to make inferences regarding the fracture regime in the study area.

Chapter 6

Conclusions

6.1 Conclusions

We can conclude that the composite attribute performs efficaciously. The case studies show that the attribute effectively picks complicated faulting and it appears to be an improvement over commonly used attributes.

The composite attribute is compared to these attributes and it appears to outperform them. Common attributes (like coherence and curvature) do an excellent job when determining fault extent, but their windowing effect is noticeable in vertical section. The composite attribute has excellent vertical resolution. The use of the phase spectra from spectral decomposition allows us to observe smaller changes in the behavior of faults, which is later translated in better fault characterization both laterally and vertically.

The validation tests were successful as well. The composite attribute is able to detect faults at well log scale. It is also able to maintain lateral fault connectivity, not disrupting fault planes, as it is shown in the co-rendering example.

Both, the models and the field tests, show that the attribute is highly affected by the presence of noise. Data conditioning can improve signal to noise ratio, and therefore the attribute's response.

References

Browaeys, T. J, 2009, Complex-valued correlation and seismic attributes: SEG Expanded Abstracts 28, 1053-1057.

Castagna, J.P. and S. Sun, 2003, Instantaneous spectral analysis: Detection of low-frequency shadows associated with hydrocarbons: The Leading Edge 22, 120-127.

Castagna, J. P. and S. Sun, 2006, Comparison of spectral decomposition methods: EAGE, First break, Volume 24, Technology Feature, 75-79.

Caughey, C., 1977, Depositional Systems in the Paluxy Formation (Lower Cretaceous), Northeast Texas-Oil, Gas, and Groundwater Resources: Bureau of Economic Geology, the University of Texas at Austin, No. 77-8.

Chopra, S., and K. Marfurt, 2008, Seismic Attributes for Prospect Identification and Reservoir Characterization: SEG Geophysical Developments Series No. 11.

Guo, H., K. Marfurt, and J. Liu, 2009, Principal component spectral analysis: Geophysics, 74, P35-P43.

Jackson, M. P., 1982, Fault Tectonics of the East Texas Basin: Bureau of Economic Geology, The University of Texas at Austin, No. 82-4.

Jansen, K., 2005, Seismic Investigation of Wrench Faulting and Fracturing At Rulison Field, Colorado (Master's Thesis), Colorado School Of Mines, Boulder, CO.

Levey, R., B. Hardage, R. Edson, and V. Pendleton, 1994, 3D Seismic and Well Log Data Set, Fluvial Reservoir Systems—Stratton Field, South Texas: Bureau of Economic Geology, the University of Texas Austin.

Liner, C., 2004, Synthetic Seismogram, Tuning, and Resolution: Elements of 3D Seismology, Second Edition, Chapter 20, 411-412.

Luo, Y., W. G. Higgs, and W. S. Kowalik, 1996: Edge detection and stratigraphic analysis using 3D seismic data, SEG Expanded Abstracts 15, 324-327.

Matos, M. C., O. Davogusto, K. Zhang, and K. Marfurt, 2010, Continuous wavelet transform phase residues applied to detect stratigraphic discontinuities: SEG Expanded Abstracts 29, 1494-1499.

Natural Central University., 2005, Basin Research Group, http://140.115.21.141/html/index.htm, accessed 9 November 2012.

Partyka, G., J. Gridley, and J. Lopez, 1999, Interpretational applications of spectral decomposition in reservoir characterization: The Leading Edge 18, 353-360.

Petroleum Exploration Society of Australia, 2001, New Direction For Novus: International News, Oct/Nov, www.pesa.com.au.

Peyton, L., R. Bottjer, and G. Partyka, 1998, Interpretation of incised valleys using new 3-D seismic techniques: A case history using spectral decomposition and coherency: The Leading Edge 17, 1294-1298.

Pujol, J., 2003, Introduction to Tensors and Dyadics: Elastic Wave Propagation and Generation in Seismology, Chapter 3, 19-20.

Puryear, C., O. Portniaguine, C. Cobos, and J. P. Castagna, 2012, Constrained Least Squares Spectral Analysis: Application to seismic data: Geophysics, Volume 77, No 5, V143-V167.

Randen, T., S. I. Pedersen, and L. Pedersen, 2011, Automatic extraction of fault surfaces from three-dimensional seismic data: SEG Int'l Exposition and Annual Meeting.

Taner, M. T., F. Koehler, and R. E. Sheriff, 1979, Complex seismic trace analysis: Geophysics, 44, No 6, 1041-1063.

Taner, T, 1992, Attributes Revisited: OHM Rock Solid Images. http://rocksolidimages.com/pdf/attrib_revisited.htm.

Zhou, Y., J. Gao, and W. Chen, 2007, Local structural entropy based on frequency-division instantaneous phase for enhancing seismic discontinuities: SEG Expanded Abstracts 26, 846-850.